June 2012 / version 1.0

The $\bar{p}p \to l^+l^-$ and $\bar{p}p \to \pi^+\pi^-$ cross section

Manuel Zambrana[1], Dmitry Khaneft[2], Bertalan Feher, Christina Haberkorn, Paul Larin, Pascal Lautz, Dexu Lin, Yue Ma, Frank Maas, María del Carmen Mora, Cristina Morales, Roberto Pérez, David Rodríguez and Iris Zimmermann

in collaboration with J. Van de Wiele[a] and S. Ong[b]

Institut für Kernphysik, University of Mainz, Becher Weg 45, D-55128 Mainz
Helmholtz Institute Mainz, University of Mainz, D-55128 Mainz

[a] Institut de Physique Nucléaire, IN2P3-CNRS, Université de Paris-Sud, 91406 Orsay Cedex, France
[b] Université de Picardie Jules Verne, F-80000 Amiens, France

Abstract

In this note we describe the differential cross section for the processes $\bar{p}p \to l^+l^-$, with $l = e, \mu$ or τ, and $\bar{p}p \to \pi^+\pi^-$, when both the proton target and the antiproton beam and the antiproton beam are unpolarized. For lepton production, the cross section is a leading order calculation with a massive lepton in the final state. For pion production, the parametrization of the cross section in the low energy regime is based on a Legendre polynomial fit to data from the (antiproton beam) CERN 28 GeV proton synchroton, whereas in the high energy regime the recent predictions by J. van de Wiele and S. Ong based on a Regge Theory approach were used. A computer code to perform integration of both the lepton and pion cross section in a user-defined kinematic region is also described.

[1]email: zambrana@kph.uni-mainz.de
[2]email: khaneftd@kph.uni-mainz.de

Contents

1 Introduction

The availability of a high-intensity antiproton beam up to 15 GeV at the FAIR facility and of the PANDA detector offers unique possibilities for new investigations of the hadron structure (see [1] for a review). Feasibility studies for the determination of the proton electromagnetic form factors in the time-like region [2] with the PANDA detector have been already performed through the annihilation process $\bar{p}p \to l^+l^-$, with $l = e$ or μ, at several antiproton beam energies [3]. The difficulty of the measurement is related to the hadronic background, mostly annihilation into pions, which is estimated to be about six orders of magnitude larger than the production of the lepton pair. The development of efficient algorithms for signal reconstruction and background rejection requires the use of Monte Carlo event generators for both lepton and pion production based on realistic input cross sections at the true-level. Moreover, realistic simulation studies require the use of the expected statistics for a given nominal luminosity, so the integration (analytical or numerical) of a realistic differential cross section in the kinematic region of the measurement is needed. In this note we describe the differential cross section for the processes $\bar{p}p \to l^+l^-$, with $l = e, \mu$ or τ, and $\bar{p}p \to \pi^+\pi^-$, when both the proton target and the antiproton beam and the antiproton beam are unpolarized. For lepton production, the cross section is a leading order calculation with a massive lepton in the final state [4]. For pion production, the parametrization of the cross section in the low energy regime is based on a Legendre polynomial fit to data from the (antiproton beam) CERN 28 GeV proton synchroton [5], whereas in the high energy regime the recent predictions by J. van de Wiele and S. Ong [6] based on a Regge Theory approach were used. In those regions of the phase space not covered by the data or where the theoretical predictions are not expected to be reliable, an interpolated cross section was first obtained using the available inputs. The continuous antiproton momentum range from 0.79 GeV to 12.0 GeV in the LAB frame was fully covered in this way. A computer code to perform the integration of the differential cross section for both lepton and pion production in a user defined kinematic region is also described.

2 Conventions

Throughout this note, natural units $\hbar = c = 1$ are used. The components p^μ of a generic four-momentum p are labelled by the integer index μ, which takes the values $\mu = 0, 1, 2, 3$. The temporal componet p^0 refers to the energy E and the spatial components p^i, with $i = 1, 2, 3$,

to the 3-dimensional part $\mathbf{p}$ of the four-momentum. Therefore, we write $p = (E, \mathbf{p})$. The Minkowski metric with signature $g = \mathrm{diag}(+,-,-,-)$ is used. With this choice, the square of the four-momentum becomes $p^2 = p^T\, g\, p = E^2 - \mathbf{p}^2$, where the superscript T stands for matrix transpose. On-shell particles therefore satisfy the relation $p^2 = E^2 - \mathbf{p}^2 = m^2$, where m is the mass of the particle.

3 The $\bar{p}p \to l^+l^-$ differential cross section

The differential cross section for the annihilation process $\bar{p}(p_1)\ p(p_2) \to l^+(p_3)\ l^-(p_4)$ was first obtained in ref [4], and later on recalculated [7]. At the lowest order, the proccess occurs through the so called *one photon exchange* (OPE) mechanism, that is, the annihilation of the initial hadron state $\bar{p}p$ into a virtual photon γ^* which then decays to the lepton pair l^+l^- observed in the final state. The only diagram which contributes to the tree-level scattering amplitude is shown in Fig 1.

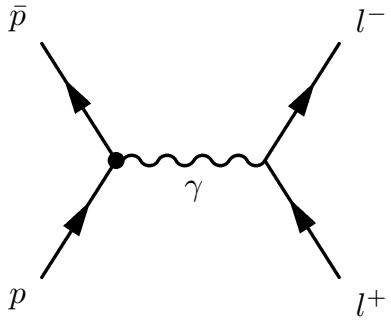

Figure 1: *LO contributing diagram to* $\bar{p}p \to l^+l^-$

Four-momentum conservation at the hadronic vertex implies that the four-momentum squared q^2 carried by the virtual photon is given, at the lowest order, by

$$q^2 = (p_1 + p_2)^2 = s\ , \tag{3.1}$$

where s is the $\bar{p}p$ center of mass energy squared. At this order of approximation and keeping in the calculation the mass of the final state lepton m_l, the differential cross section per unit of $\cos\theta^*$, where θ^* is defined as the polar angle of the negative charged lepton measured with respect the anti-proton direction in the $\bar{p}p$ center of mass frame, is given by

$$\frac{d\sigma}{d\cos\theta^*} = \frac{\pi\alpha^2}{2s}\ \frac{\beta_l}{\beta_p}\ \left\{ \left(2 - \beta_l^2 + \beta_l^2\cos^2\theta^*\right)|G_M|^2 + \frac{1}{\tau}\left(1 - \beta_l^2\cos^2\theta^*\right)|G_E|^2 \right\}\ , \tag{3.2}$$

where $|G_E|$ and $|G_M|$ are the modulus of the (Sachs) electric and magnetic proton form factors (FFs), respectively, evaluated at $q^2 = s$, and where the kinematic factors β_l, β_p and τ are given by

$$\beta_l = \sqrt{1 - 4m_l^2/s} \tag{3.3}$$

$$\beta_p = \sqrt{1 - 4M^2/s} \tag{3.4}$$

$$\tau = \frac{q^2}{4M^2} \, , \tag{3.5}$$

with M the mass of the proton.

The threshold $s > 4M^2 > 4m_{e,\mu}^2$ ensures that electron and muon production is always possible at any value of proton-antiproton center of mass energy. Tau production starts only at $s > 4m_\tau^2$. In the case of electron production, terms of the order $(m_e/M)^2 \sim 10^{-7}$ can be safely neglected by formally setting $m_l = 0$, or $\beta_l = 1$, in Eq. 3.2, which then becomes

$$\frac{d\sigma}{d\cos\theta^*} = \frac{\pi\alpha^2}{2s} \, \frac{1}{\beta_p} \, \left\{ \left(1 + \cos^2\theta^*\right) |G_M|^2 + \frac{1}{\tau}(1 - \cos^2\theta^*)|G_E|^2 \right\} \quad . \tag{3.6}$$

In our numerical implementation, only the full cross section given by Eq. 3.2 is used for electron, muon and tau production, even when Eq. 3.6 could be taken as an accurated approximation in the case of electron production.

4 Models for the form factors

The evaluation of the cross section 3.2 requires the knowledge of the form factors in the time-like region (TL), that is, for $q^2 > 0$. For numerical estimates, a number of different models have been considered.

4.1 Dipole-modified model

In the space-like (SL) region, the existing data are described by a dipole behavior up to the highest masured value $Q^2 = -q^2 \sim 31$ GeV^2 [8], according to the real functions

$$G_M(Q^2)/\mu = G_d(Q^2), \qquad G_d(Q^2) = (1 + Q^2/m_d^2)^{-2} \, , \tag{4.1}$$

where $\mu \sim 2.79$ is the proton anomalous magnetic moment and $m_d^2 \sim 0.71$ GeV^2.

In the TL region, the magnetic form factor of the proton can be parametrize as

$$|G_M(q^2)| = a\ G_d(-Q^2)\ (1 + q^2/m_{nd}^2)^{-1} = a\ (1 + q^2/m_d^2)^{-2}\ (1 + q^2/m_{nd}^2)^{-1}\ , \qquad (4.2)$$

where $a = 22.5$ is a normalization parameter obtained from a fit to TL data and $m_{nd} = 3.6$ GeV^2 characterizes the deviation from the usual dipole q^2-dependence.

4.2 Perturbative QCD-inspired model

A perturbative QCD-inspired parametrization of both $|G_E|$ and $|G_M|$ can be obtained by analytical continuation of the dipole form factor 4.1 to the TL region, with the replacement $Q^2 \to q^2$. Corrections based on dispersion relations have been suggested in [9] to avoid "ghost" poles in the strong coupling constant α_s, and can be included in the following form:

$$|G_E(q^2)| = |G_M(q^2)| = \frac{D}{q^4\left[\log^2(q^2/\Lambda^2) + \pi^2\right]}\ , \qquad D = 89.45\ \text{GeV}^2\ , \qquad (4.3)$$

where the normalization constant D is obtained by fitting the experimental data and $\Lambda = 0.3$ is the QCD scale parameter.

4.3 Vector meson dominance

A semi-phenomenological model of the nucleon in the SL region in which the external photon couples to both an intrinsic structure, described by the form factor $g(Q^2)$, and a meson cloud, treated within the framework of vector meson dominance (ρ, ω, φ), was suggested [10]. The analytical continuation of this model to the TL region $q^2 > 4m_\pi^2$ was performed in [11], and the isoscalar and isovector parts of the Dirac and Pauli form factors were parametrized as

$$
\begin{aligned}
F_1^S(q^2) &= \frac{1}{2}g(q^2)\Big\{(1-\beta_\omega-\beta_\varphi)+\beta_\omega P_\omega(q^2)+\beta_\varphi P_\varphi(q^2)\Big\} \\
F_1^V(q^2) &= \frac{1}{2}g(q^2)\Big\{(1-\beta_\rho)+\beta_\rho P_\rho(q^2)\Big\} \\
F_2^S(q^2) &= \frac{1}{2}g(q^2)\Big\{(-0.120-\alpha_\varphi)P_\omega(q^2)+\alpha_\varphi P_\varphi(q^2)\Big\} \\
F_2^V(q^2) &= \frac{1}{2}g(q^2)\Big\{3.706\ P_\rho(q^2)\Big\} \quad , \qquad (4.4)
\end{aligned}
$$

where the intrinsic form factor $g(q^2)$ and the propagator terms $P_\omega(q^2)$, $P_\varphi(q^2)$ and $P_\rho(q^2)$ are given by the expressions

$$
\begin{aligned}
g(q^2) &= \frac{1}{(1-\gamma\ e^{i\theta}\ q^2)} \\
P_\omega(q^2) &= \frac{m_\omega^2}{m_\omega^2-q^2} \\
P_\varphi(q^2) &= \frac{m_\varphi^2}{m_\varphi^2-q^2} \\
P_\rho(q^2) &= \frac{m_\rho^2+8\Gamma_\rho m_\pi/\pi}{m_\rho^2-q^2+(4m_\pi^2-q^2)\Gamma_\rho\alpha(q^2)/m_\pi+i\Gamma_\rho 4m_\pi\beta(q^2)} \quad , \qquad (4.5)
\end{aligned}
$$

with functions $\alpha(q^2)$ and $\beta(q^2)$ defined as

$$
\begin{aligned}
\alpha(q^2) &= \frac{2}{\pi}\left[\frac{q^2-4m_\pi^2}{q^2}\right]^{1/2}\ln\left(\frac{\sqrt{q^2-4m_\pi^2}+\sqrt{q^2}}{2m_\pi}\right) \\
\beta(q^2) &= \sqrt{\left(\frac{q^2}{4m_\pi^2}-1\right)^3\Big/\left(\frac{q^2}{4m_\pi^2}\right)}\ . \qquad (4.6)
\end{aligned}
$$

The parametrization uses coupling constants with values $\beta_\rho = 0.672$, $\beta_\omega = 1.102$, $\beta_\varphi = 0.112$ and $\alpha_\varphi = -0.052$, an intrinsic form factor with $\gamma = 0.25$ GeV^{-2} and phase $\theta = 53$ deg for analytical continuation obtained by fitting the existing data. Standard values of the masses ($m_\rho = 0.765$ GeV, $m_\omega = 0.784$ GeV and $m_\varphi = 1.019$ GeV) and a ρ with $\Gamma_\rho = 0.112$ GeV were used.

The Pauli and Dirac form factors F_1 and F_2 can then be calculated by adding isoscalar and isovector parts separately:

$$\begin{aligned} F_1(q^2) &= F_1^S(q^2) + F_1^V(q^2) \\ F_2(q^2) &= F_2^S(q^2) + F_2^V(q^2) \ , \end{aligned} \tag{4.7}$$

from where the Sachs form factors G_E and G_M follow as

$$\begin{aligned} G_E(q^2) &= F_1(q^2) + F_2(q^2) \\ G_M(q^2) &= F_1(q^2) + \tau F_2(q^2) \ . \end{aligned} \tag{4.8}$$

For numerical implementations involving the unphysical region $q^2 < 4M^2$, the model has the disadvantage of becoming singular at $q^2 = m_\omega^2$ and $q^2 = m_\varphi^2$, due to the poles in the propagators $P_\omega(q^2)$ and $P_\varphi(q^2)$. Regularization and subsequent removal of the divergencies was achieved by introducing an ω and a ϕ meson with non-zero width, and therefore modifying the propagators $P_\omega(q^2)$ and $P_\varphi(q^2)$ according to

$$\begin{aligned} P_\omega(q^2) &= \frac{m_\omega^2}{m_\omega^2 - q^2} \to \frac{m_\omega^2}{m_\omega^2 - q^2 + i m_\omega \Gamma_\omega} \\ P_\varphi(q^2) &= \frac{m_\varphi^2}{m_\varphi^2 - q^2} \to \frac{m_\varphi^2}{m_\varphi^2 - q^2 + i m_\varphi \Gamma_\varphi} \ , \end{aligned} \tag{4.9}$$

with standard values $\Gamma_\omega = 0.00849$ GeV and $\Gamma_\varphi = 0.00426$ GeV [12]. The regularization scheme removes the divergencies for real values of q^2, displacing the poles to the complex values $q^2 = m_\omega^2 + i m_\omega \Gamma_\omega$ and $q^2 = m_\varphi^2 + i m_\varphi \Gamma_\varphi$, respectively. A comparison of $|G_E(q^2)|$ and $|G_M(q^2)|$ in a region containing the values $q^2 = m_\omega^2$ and $q^2 = m_\varphi^2$ for the model with and without removal of the divergencies is shown in Fig 2. From now on, when we refer to the vector meson dominance (vmd) model, we will assume that the divergencies associated to the singular propagators have been removed according to the regularization procedure just described. The ratio $|G_E(q^2)|/|G_M(q^2)|$ predicted by the vmd model is shown in Fig. 3.

Fig. 4 shows a comparison of both $|G_E(q^2)|$ and $|G_M(q^2)|$ according to the dipole-modified, perturbative QCD-inspire and vector meson dominance model, respectively.

5 The differential $\bar{p}p \to \pi^+\pi^-$ cross section

Currently, there is no single description for the $\bar{p}(p_1)\ p(p_2) \to \pi^+(p_3)\ \pi^-(p_4)$ differential cross section which is valid in the full kinematic range. For this reason, the parametrisation of the cross section was considered independently in different kinematic regions according to the data and theoretical predictions available in each case. Attending to the antiproton beam momentum in the LAB frame P, three main regions are distinguished: the *low energy region*, the *transition region* and the *high energy region*.

The low energy region

In the LAB frame (i.e. the frame in which the antiprton target is at rest) antiproton momentum range $0.79 \leq P \leq 2.43$ GeV, data from the CERN 28 GeV proton synchrotron [5] were used to parametrise the cross section. The differential cross section per unit of solid angle $d\sigma/d\Omega$ in the $\bar{p}p$ center of mass frame, where the solid angle element is defined in the usual way as $d\Omega = d\cos\theta^* d\phi^*$, with θ^* the angle between the negative charged pion and incoming antiproton, was measured for 20 incident momenta of the antiproton beam as a function of $\cos\theta^*$, covering the angular range $|\cos\theta^*| < 0.94$ in a total of 48 bins.

Following the authors, at each momentum the data were fitted with a Legendre polynomial series:

$$\frac{d\sigma}{d\Omega} = \sum_{n=0}^{n_{\max}} a_n\, P_n(\cos\theta^*)\ , \tag{5.1}$$

where P_n is the Legendre polynomial of order n and the coeficients a_n are taken as the free parameters of the fit. At the highest momentum, several orders of fit were examined. The number of terms in the series was increased until there was no significant improvement in the χ^2 per degree of freedom, which then plateaued at a value closed to unity. For consistency, the same number of terms was then used throughout the momentum range, even though the cross section at lower momenta could be fitted adequately with fewer terms. Coeficients up to a_{10} were used. The fitted cross section are plotted at each of the incident momenta in Fig 5.

For reasons that will become clear later, at the highest antiproton momentum $P = 2.43$ GeV, the cross section $d\sigma/dt$, where t is the Mandelstam variable $t = -(p_1 - p_4)^2$, was calculated from the corresponding $d\sigma/d\Omega$. The mapping from $\cos\theta^*$ to t can be obtained by expanding

the squared in the CM frame:

$$\begin{aligned} t &= -(p_1 - p_4)^2 \\ &= -(p_1 + p_4 - 2p_1 \cdot p_4) \\ &= -(M^2 + m_\pi^2 - 2\,E_1 E_4 + 2|\mathbf{p_1}||\mathbf{p_4}|\cos\theta^*) \ . \end{aligned} \tag{5.2}$$

In the CM frame, each particle in the initial $\bar{p}p$ state and each particle in the final $\pi^+\pi^-$ state takes, due to the equality of their masses, half of the total available energy:

$$E_1 = E_2 = E_3 = E_4 = \sqrt{s}/2 \ , \tag{5.3}$$

which fixes the values of their momenta:

$$\begin{aligned} |\mathbf{p_1}| = |\mathbf{p_2}| &= \sqrt{\left(\frac{\sqrt{s}}{2}\right)^2 - M^2} = \sqrt{\frac{s}{4} - M^2} \\ |\mathbf{p_3}| = |\mathbf{p_4}| &= \sqrt{\left(\frac{\sqrt{s}}{2}\right)^2 - m_\pi^2} = \sqrt{\frac{s}{4} - m_\pi^2} \ . \end{aligned} \tag{5.4}$$

Differentiation of Eq. 5.2 yields the relation between $\cos\theta^*$ and t-bins:

$$dt = C\ d(\cos\theta^*) \ , \qquad C = 2|\mathbf{p_1}||\mathbf{p_4}| = 2\sqrt{\left(\frac{s}{4} - M^2\right)\left(\frac{s}{4} - m_\pi^2\right)} \ . \tag{5.5}$$

The relation between the cross section per unit of t and the cross section per unit of solid angle is then given after integrating in the azimuthal variable ϕ^*:

$$\frac{d\sigma}{dt} = \frac{1}{C}\ \frac{d\sigma}{d(\cos\theta^*)} = \frac{1}{C}\int_0^{2\pi} d\phi^*\ \frac{d\sigma}{d(\cos\theta^*)d\phi^*} = \frac{2\pi}{C}\ \frac{d\sigma}{d\Omega} \ . \tag{5.6}$$

At the highest momentum $P = 2.43$ GeV, the constant factor $2\pi/C$ takes the value 2.77 GeV^{-2}, as follows from the definition in Eq. 5.5 and the relation $s = 2M^2 + 2M\sqrt{M^2 + P^2}$.

The high energy region

In the antiproton momentum range $5.0 \leq P \leq 12.0$ GeV, the very recent predictions by J. Van de Wiele and S. Ong were used to parametrise the cross section [6]. Their Regge-inspired phenomenological model, based on the trajectories exchanged in the t and u channels, is expected to be valid at large values of the center of mass energy squared s. The comparison between the differential cross sections predictions and the available data [13, 14, 15] is done to determine the values of the few parameters of the model. Numerical values of $d\sigma/dt$ were

provided by the authors at 15 incident momenta of the antiproton beam as a function of $\cos\theta^*$ [16]. The lattice spacing in momentum was 0.5 GeV and the lattice spacing in $\cos\theta^*$ was 0.01.

The transition energy region

In the antiproton momentum range $2.43 < P < 5.0$ GeV no data were available to parametrise the cross section by an appropiate fit or to constrain the parameters of a phenomenological model. The Regge theory approach used in the high energy region was extrapolated from antiproton momentum 5.0 GeV down to 3.0 GeV, limit in which its predictions are not expected to be valid any more. In a similar way, numerical values of $d\sigma/dt$ were provided by the authors at 4 incident momenta of the antiproton beam in this range, as a function of $\cos\theta^*$ [16]. As in the previous case, lattice spacing in momentum was 0.5 GeV and the lattice spacing in $\cos\theta^*$ was 0.01. The momentum range $2.43 < P < 3.0$ GeV left a gap where no data or theoretical predictions were available. In Fig. 6, the differential cross sections $d\sigma/dt$ are plotted for 19 values of incident antiproton momenta, covering part of the transition energy region, from to $P = 3.0$ GeV, and the full high energy region, up to $P = 12.0$ GeV.

The cross section in the full $(P, \cos\theta^*)$ plane

According to the description just given, an input value for either $d\sigma/d\Omega$ or $d\sigma/dt$ (from data or from theoretical prediction) was available only at particular values of antiproton beam momentum P and $\cos\theta^*$. In those points $(P, \cos\theta^*)$ without an input cross section, linear nearest neighbor interpolation was applied to extract a value. In the momentum range $2.43 < P < 3.0$ GeV, the cross section $d\sigma/dt$ at both extremes was used cosistently to do the interpolation at momentum values in between. With this procedure, a value for the cross section $d\sigma/d\Omega$ is available in the region $0.79 \leq P \leq 2.43$ GeV and $-1 \leq \cos\theta^* \leq 1$, and a value for the cross section $d\sigma/dt$ is available in the region $2.43 < P \leq 12.0$ GeV and $-1 \leq \cos\theta^* \leq 1$. The transformation both cross sections to $d\sigma/d\cos\theta^*$ is done as follows. In the momentum range $0.79 \leq P \leq 2.43$ GeV, the cross section per unit of solid angle $d\sigma/d\Omega$ is integrated in the azimuthal variable ϕ^*:

$$\frac{d\sigma}{d\cos\theta^*} = \int_0^{2\pi} d\phi^* \, \frac{d\sigma}{d\Omega} = 2\pi \, \frac{d\sigma}{d\Omega} \, , \tag{5.7}$$

whereas in the momentum range $2.43 < P \leq 12.0$ GeV, the transformation of $d\sigma/dt$ to

$d\sigma/d\cos\theta^*$ reads

$$\frac{d\sigma}{d\cos\theta^*} = C\ \frac{d\sigma}{dt}\ , \tag{5.8}$$

where the factor C, defined in Eq. 5.5, is evaluated at the center of mass energy squared $s = 2M^2 + 2M\sqrt{M^2+P^2}$.

6 The $\bar{p}p \to l^+l^-$ integrated cross section

The cross section given by Eq. 3.2 can be rewritten in the form

$$\frac{d\sigma}{dx} = A_1\ (A_2 + A_3\ x^2)\ , \tag{6.1}$$

where we have changed variables to $x \equiv \cos\theta^*$ and the factors A_1, A_2 and A_3 are given by

$$\begin{aligned} A_1 &= \frac{\pi\alpha^2}{2}\ \frac{\beta_l}{s\beta_p} \\ A_2 &= (2-\beta_l^2)|G_M|^2 + \frac{1}{\tau}|G_E|^2 \\ A_3 &= \beta_l^2\left(|G_M|^2 - \frac{1}{\tau}|G_E|^2\right)\ . \end{aligned} \tag{6.2}$$

The integration in the angular range $a < x < b$ can be done analytically in a strightforward way:

$$\sigma = \int_a^b dx\ \frac{d\sigma}{dx} = A_1\left[A_2(b-a) + \frac{1}{3}A_3(b^3-a^3)\right]\ . \tag{6.3}$$

In case the full angular range $-1 < x < 1$ is covered in the integration region, the previous result becomes

$$\sigma_T = 2A_1\left[A_2 + \frac{1}{3}A_3\right]\ . \tag{6.4}$$

Fig. 7 shows, as a function of the center of mass energy s, the result of integrating of the differential cross section $d\sigma/d\cos\theta^*$ in the full angular range $-1 < \cos\theta^* < 1$ for electron, muon and tau production, assuming the form factors $G_E(q^2)$ and $G_M(q^2)$ given by the pQCD-inspired model.

7 The $\bar{p}p \to \pi^+\pi^-$ integrated cross section

In the abstence of an analytical description, the integration of $d\sigma/d\cos\theta^*$ for pion production requires the use of numerical methods.

Let us recall that the mean value of a function f of a single variable x in the interval $a < x < b$ is defined as

$$\langle f \rangle = \frac{I}{L} \ , \qquad L = b - a \ , \qquad I = \int_a^b dx \ f(x) \ . \tag{7.1}$$

The previous equation can be solved to compute the integral I as

$$I = L \ \langle f \rangle \ , \tag{7.2}$$

provided that the mean value $\langle f \rangle$ is calculated by some other method. The simplest Monte Carlo technique to calculate $\langle f \rangle$ consists of doing uniform sampling of the variable x in the interval $a < x < b$. An estimate of $\langle f \rangle$, is then given by

$$\overline{f} = \frac{1}{N} \sum_{i=1}^{N} f(x_i) \ , \tag{7.3}$$

where N is the total number of points in the sample $\{x_i\}$. The estimate and standard deviation for the integral are then given by [1]

$$\begin{aligned} I &\sim L \cdot \overline{f} \\ \Delta I &\sim L \sqrt{\frac{1}{N-1} (\overline{f^2} - \overline{f}^2)} \ , \end{aligned} \tag{7.4}$$

where the squared mean value $\overline{f^2}$ is defined as

$$\overline{f^2} = \frac{1}{N} \sum_{i=1}^{N} f(x_i)^2 \ . \tag{7.5}$$

The $\bar{p}p \to \pi^+\pi^-$ differential cross section has been numericaly integrated using this technique, taking $d\sigma/d\cos\theta^*$ as the function f and the integration variable $\cos\theta^* = x$, keeping the antiproton momentum P as a parameter. Fig. 8 shows the integrated pion cross section in the angular region $-1 < \cos\theta^* < 1$ and $-0.9 < \cos\theta^* < 0.9$, as a function of the $\bar{p}p$ center of mass energy s. In the full angular region, i.e. $-1 < \cos\theta^* < 1$, the fluctuations between $s = 4.06$ GeV^2 (or $P = 0.79$ GeV) and $s = 6.65$ GeV^2 (or $P = 2.43$ GeV) are due to the large extrapolations when the Legendre polynomial fit is extended beyond $|\cos\theta^*| > 0.94$, where no data is available. Such fluctuations are suppressed when the integration region is restricted to $-0.9 < \cos\theta^* < 0.9$, as it can be seen. The "bump" between $s = 6.65$ GeV^2 (or $P = 2.43$ GeV) and $s = 7.76$ GeV^2 (or $P = 3.0$ GeV) is an effect of interpolating the cross section as a linear function of the antiproton momentum P between the two momentum

[1] for a review of the Monte Carlo methods, see, for instance, [17]

values, which gets cuadratic dependence when it is expressed as a function of the center of mass energy s. The ratio of the integrated pion and lepton (electron) cross section (in units of 10^6), as a function of the center of mass energy s, is shown in Fig. 9.

8 Numerical implementation

A computer C++ code has been developed in order to compute in the integrated lepton and pion cross section in a user-defined angular region, for a given value of the $\bar{p}p$ center of mass energy squared s, or, equivanlently, antiproton momentum P. The integration of the lepton cross section is done analytically, as described in Sec. 6. The integration of the pion cross section is done numerically, using the Monte Carlo techniques described in Sec. 7. The pseudo ramdom number generator used to produced uniformly distributed random numbers in the interval $[0, 1)$ was RANLUX [18], whose source code [19] was added to our program.

The code is organize in four pararell directories:

```
inc      src      output      plots
```

The proper code is placed in the directories `\inc` and `\src` , which contain header and source files, respectively. The output of the program is place in the directory `\output` , whereas the directory `\plots` contains a ROOT macro which produces a number of plots corresponding to the generated distributions.

Compilation of the code is done in the directory `\src` , through the sequence

```
make clean
make
```

which produces the executable `mzgen.exe`. Running the programm is actually done by execution of the script

```
./run.sh
```

Parameters are passed to the program by the infile `mzgen.in`, which can be editted, saved and the program re-run without the need of recompiling the code. In the infile `mzgen.in` the user provides the following data:

- *lepton flag*: an integer to set the final state lepton. The possible values are 0 (electron), 1 (muon) or 2 (tau).

- P: the (lab frame) antiproton momentum, in units of GeV. The allowed range is $0.79 \leq P \leq 12.0$ GeV, where the pion cross section is available. Setting a value below the PANDA threshold $P < 1.5$ GeV is possible, but a warning message will be printed out to the log file.

- $\cos\theta^*_{min}$ and $\cos\theta^*_{max}$: minimum and maximum values, respectively, of $\cos\theta^*$. The allowed range is $-1 \leq \cos\theta^*_{min} < \cos\theta^*_{max} \leq 1$. However, for antiproton momentum in the interval $0.79 < P < 2.43$ GeV (i.e. the low energy region), it is recomended to limit the angular range to $-0.94 < \cos\theta^*_{min} < \cos\theta^*_{max} < 0.94$, as in this range the pion cross section in the very forward or very backward angles might be affected by large extrapolations resulting from extending the fit function beyond the measurements range. Exceeding these limits is possible, but warning message will be printed out to the log file.

- N_{BINS}: number of bins in the $\cos\theta^*$ distributions.

- *form factor flag*: an integer to set the form factor model needed to compute the lepton cross section. The possible values are 0 (pQCD-inspire), 1 (vmd) or 2 (dipole-modified).

- $|G_E|/|G_M|$: ratio of the (Sachs) electric and magnetic proton form factors at $q^2 = s$. The allowed range is $|G_E|/|G_M| \geq 0$.

- L: luminosity, in units of fb^{-1}. Needed estimate the number of expected events in a data sample, both for lepton and pion production, for antiproton momentum P, in the kinematic region $\cos\theta^*_{min} < \cos\theta^* < \cos\theta^*_{max}$.

- *seed*: the initialisation seed fixing the state in RANLUX, an integer in the range $[1, 2^{31})$.

- N_{MC}: number of iterations in the Monte Carlo integration of the pion cross section. Setting $N_{MC} = 10^6$ should generally provide a precision better than 0.1% in the integrated pion cross section.

- *pathout*: the path to the output, relative to the `\src` directory. By default, it is set to `../output`

- *outfile*: name of the ROOT output file containing the histograms. By default, it is set to `mzhistos`.

Running the program proceeds in the following way. First, in the initialisation stage, the values of all user-defined parameters are read from the infile and checked. If any of them lies outside the allowed ranges, the job is killed and an error message is printed to the log file. Basic kinematic information, including center of mass energy squared, parametrization of the pion cross section and the need of interpolating between two antiproton momenta, is also printed to the log file, and the random number generator is initialised. Then, the calculation of the integrated cross section for both lepton and pion production is performed, first in the whole angular region $\cos\theta^*_{min} < \cos\theta^* < \cos\theta^*_{max}$ and then bin-by-bin in $\cos\theta^*$. For the lepton cross section, the values of both $|G_E(q^2)|$ and $|G_M(q^2)|$ are first taken from model, and the cross section is calculated. In addition, the lepton cross section is also recalculated by keeping the value of $|G_M(q^2)|$ as given by the FF model and setting $|G_E(q^2)|$ to the value $R \cdot |G_M(q^2)|$, where R is the user-defined ratio $|G_E|/|G_M|$. All total and bin-integrated cross sections are printed to the log file, which ends up with a short description of the histograms created and saved in the ROOT output file.

As an example, we include here the result of runninig the program with the following infile:

```
0          !  lepton, 0=electron, 1=muon, 2=tau
3.3        !  momentum pbar (GeV)
-1.0       !  cos(theta*) min
1.0        !  cos(theta*) max
10         !  #bins
0          !  FF model, 0=pQCD, 1=vmd, 2=dipole-modified
3.0        !  ratio GE/GM
2.0        !  luminosity (fb^-1)
1          !  RANLUX seed:  [1,2^31-1]
1000000    !  #MC integration points
../output  !  pathout
mzhistos   !  outfile
```

The resulting output file `output.log`, which is placed in the directory `\output`, is shown in Figs. [10-13]. In addition, the file `mzhistos.root`, which contains histograms with the calculated distributions, is created placed in the same directory. Execution of the ROOT macro `mzplots.C` in the directory `\plots` produces `.eps` files for the calculated distributions.

They are shown in Figs.[14-21].

Acknowledgements

This work has been supported by BMBF/FAIR-Panda, by Helmholtz Institute Mainz, by IPN Orsay and by GSI/IN2P3 collaboration agreement. We are indebted to J. Van de Wiele and S. Ong for providing us with their cross section predictions, as well as many useful discussions and lots of explanations. We are very grateful to Stefano Spataro and the PANDA Computing Group for their help and support with the technicalities of PandaRoot. We would also like to express our gratitude to all our colleages in IPN Orsay for their hospitality and for providing the perfect enviroment for exciting scientific discussions.

References

[1] M. F. M. Lutz *et al.* [PANDA Collaboration], *"Physics Performance Report for PANDA: Strong Interaction Studies with Antiprotons"*, [arXiv:0903.3905 [hep-ex]].

[2] E. Tomasi-Gustafsson, M. P. Rekalo, *"New possibility for further measurements of nucleon form factors at large momentum transfer in time-like region:* $\bar{p}p \to ll,\ l = e\ or\ \mu$*"*, [arXiv:0810.4245 [hep-ph]].

[3] M. Sudol *et al.*, Eur. Phys. J. A **44**, 373-384 (2010)

[4] A. Zichichi, S. M. Berman, N. Cabibbo and R. Gatto, *"Proton antiproton annihilation into electrons, muons and vector bosons"*, Nuovo Cim. **24**, 170 (1962).

[5] E. Eisenhandler *et al.*, Nuclear Physics B **96**, 109 (1975).

[6] J. Van de Wiele and S. Ong, Eur. Phys. J. A **46** (2010) 291.

[7] J. Van de Wiele and C. Morales, private communication (unpublished), (2011).

[8] R. G. Arnold, P. E. Bosted, C. C. Chang, J. Gomez, A. T. Katramatou, C. J. Martoff, G. Petratos and A. A. Rahbar *et al.*, *"Measurement of Elastic electron Scattering from the Proton at High Momentum Transfer"*, Phys. Rev. Lett. **57**, 174 (1986).

[9] D. V. Shirkov and I. L. Solovtsov, *"Analytic model for the QCD running coupling with universal alpha-s (0) value"*, Phys. Rev. Lett. **79**, 1209 (1997) [hep-ph/9704333].

[10] F. Iachello, A. D. Jackson and A. Lande, *"Semiphenomenological fits to nucleon electromagnetic form-factors"*, Phys. Lett. B **43**, 191 (1973).

[11] F. Iachello and Q. Wan, *"Structure of the nucleon from electromagnetic timelike form factors"*, Phys. Rev. C **69**, 055204 (2004).

[12] C. Amsler *et al.* [Particle Data Group Collaboration], *"Review of Particle Physics"*, Phys. Lett. B **667**, 1 (2008).

[13] A. Eide *et al.*, Nucl. Phys. B **60**, 173 (1973).

[14] T. Buran *et al.*, Nucl. Phys. B **116**, 51 (1976).

[15] C. White *et al.*, Phys. Rev. D **49**, 58 (1994).

[16] J. Van de Wiele, S. Ong and M. Zambrana, private communication (unpublished), (2010).

[17] M. H. Kalos and P. A. Whitlock, *Monte Carlo Methods*, 2nd edition, WILEY-VCH Verlag, 2008.

[18] M. Lüscher, Comp. Phys. Comm. **79** (1994) 100.

[19] available online at the author web page:
`http://luscher.web.cern.ch/luscher/ranlux/index.html`.

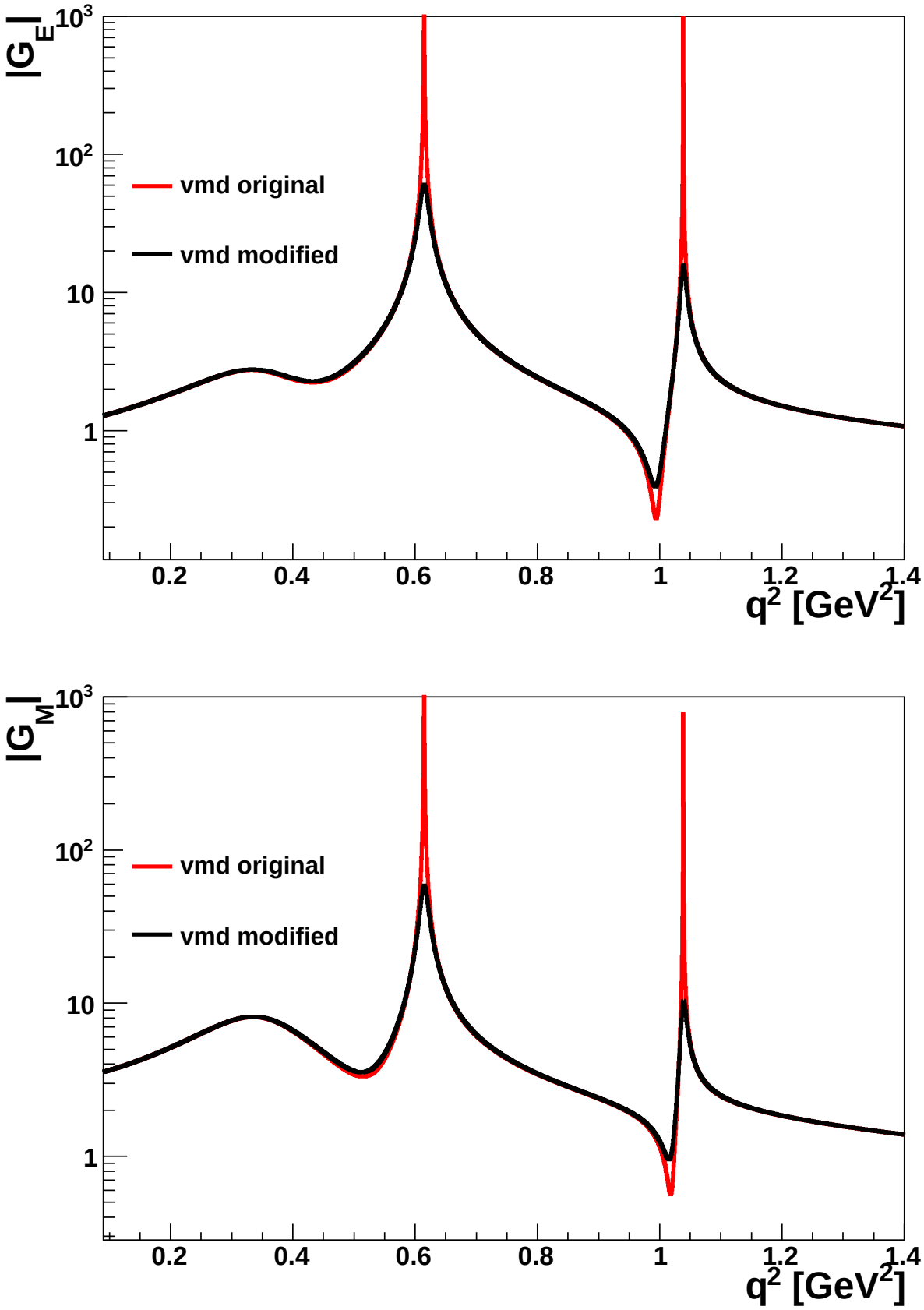

Figure 2: *A comparison of $|G_E(q^2)|$ (top) and $|G_M(q^2)|$ (down) as given by the original (red) and regularized (black) vector meson dominance model.*

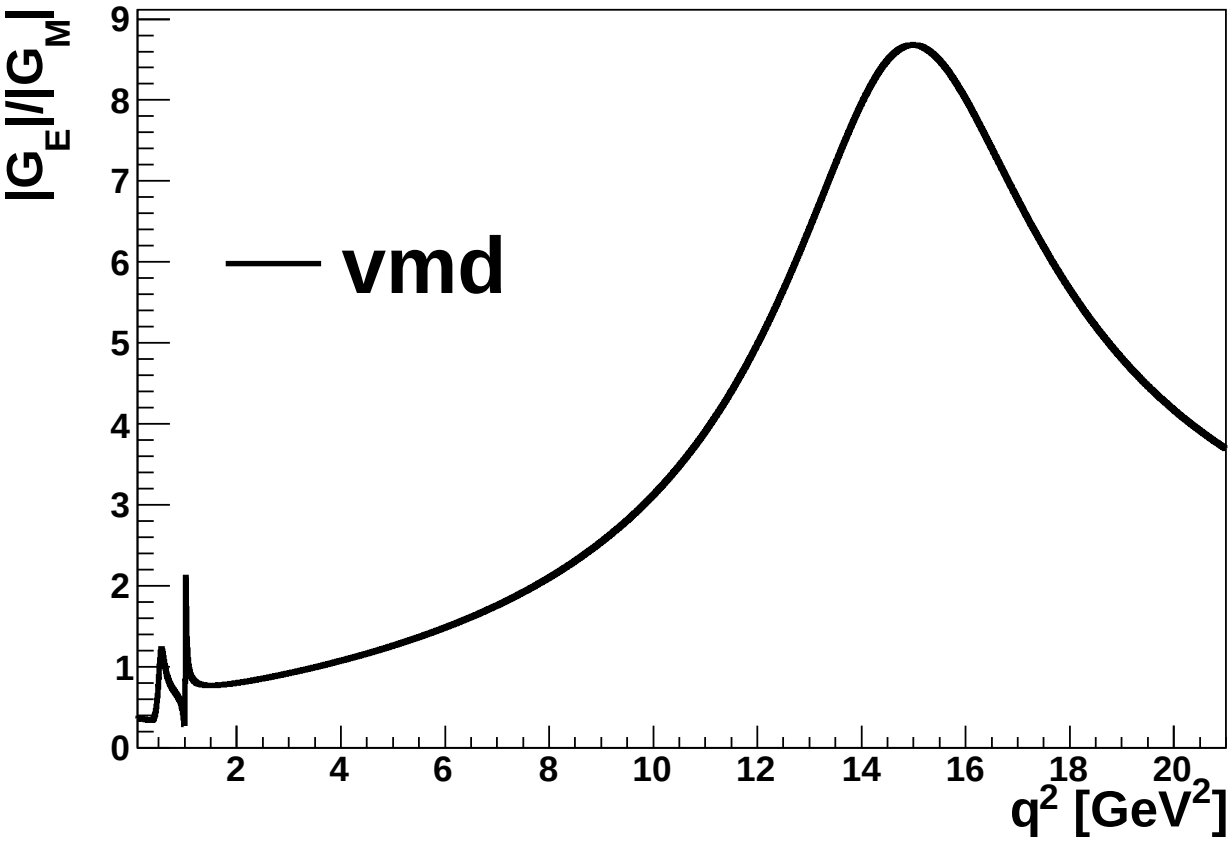

Figure 3: *The ratio $|G_E|/|G_M|$ as a function of q^2 according to the vector meson dominance model.*

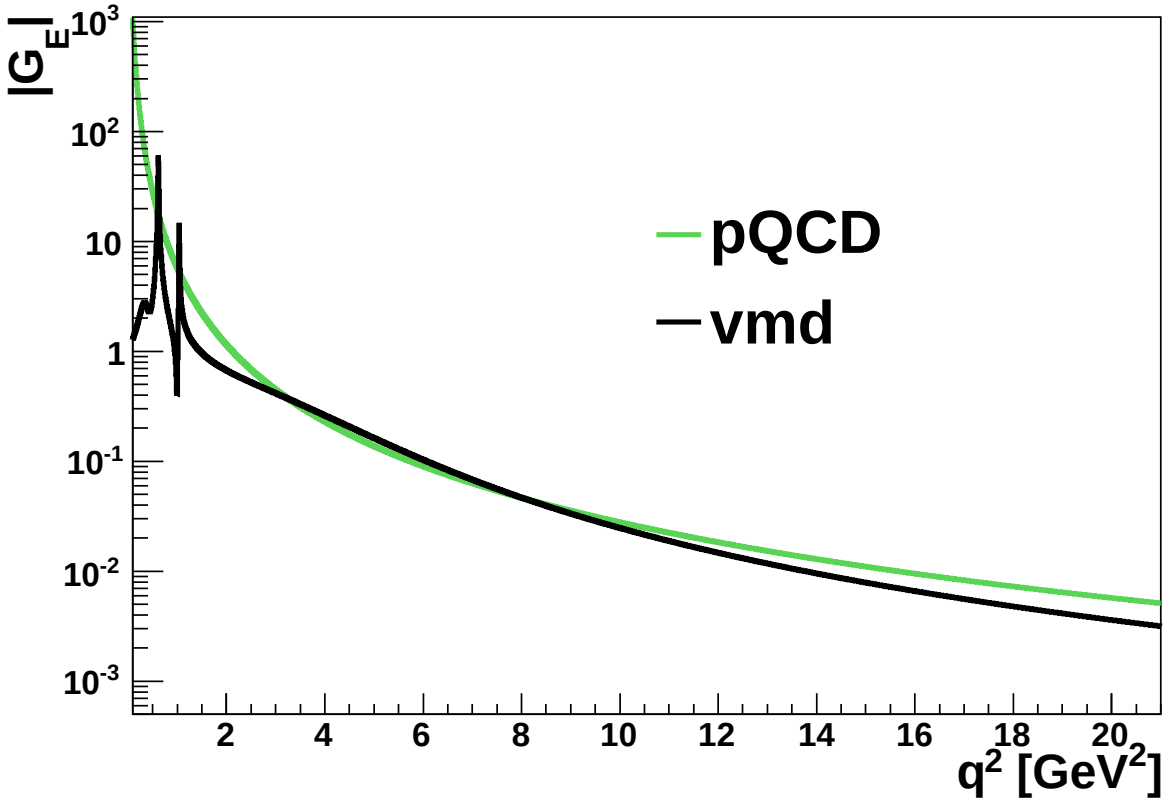

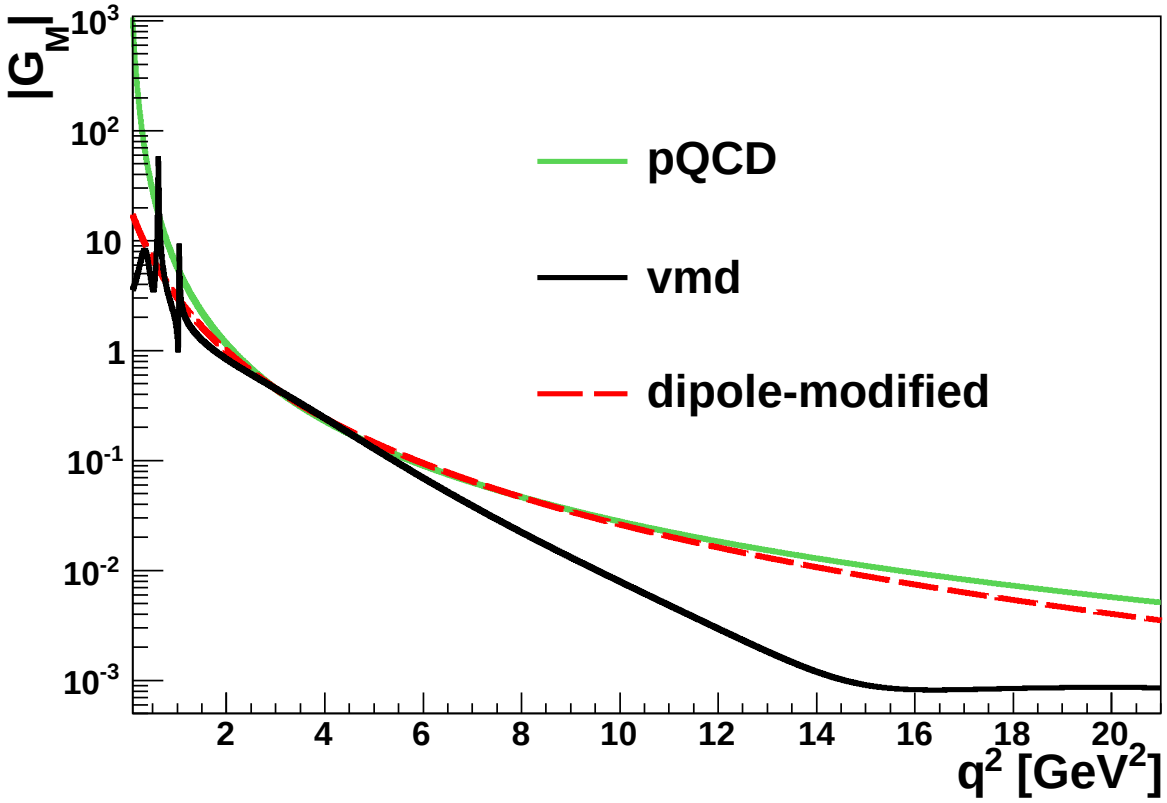

Figure 4: *The function $|G_E(q^2)|$ (top) and $|G_M(q^2)|$ (down) according to the dipole-modified (red), pertubative QCD-inspired (green) vector meson dominance (black) model, respectively.*

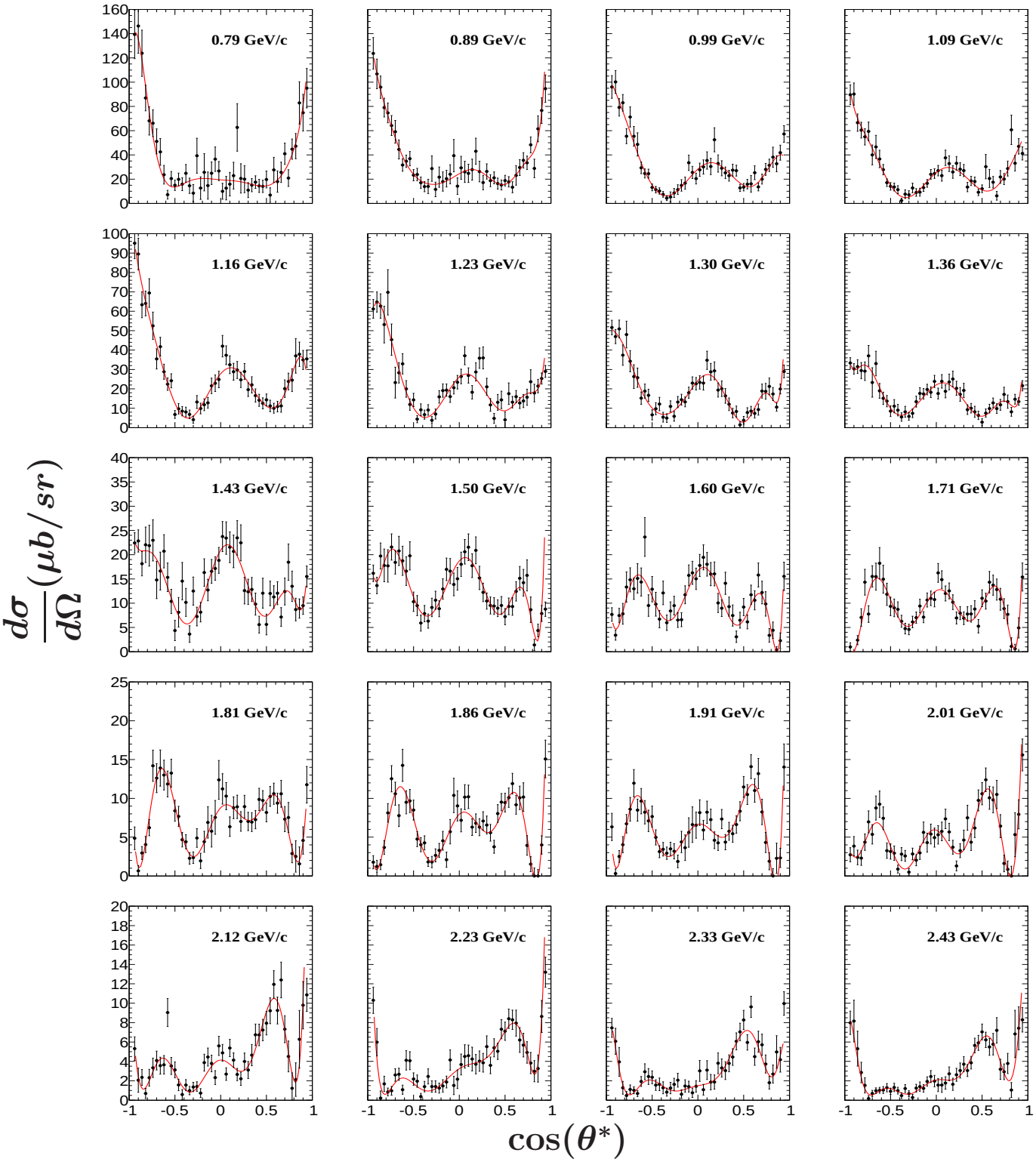

Figure 5: *Differential cross section for the process* $\bar{p}p \to \pi^+\pi^-$ *per unit of solid angle as a function of* $\cos\theta^*$ *in the* $\bar{p}p$ *center of mass frame, for antiproton momentum in the lab frame from* 0.79 *GeV to* 2.43 *GeV.*

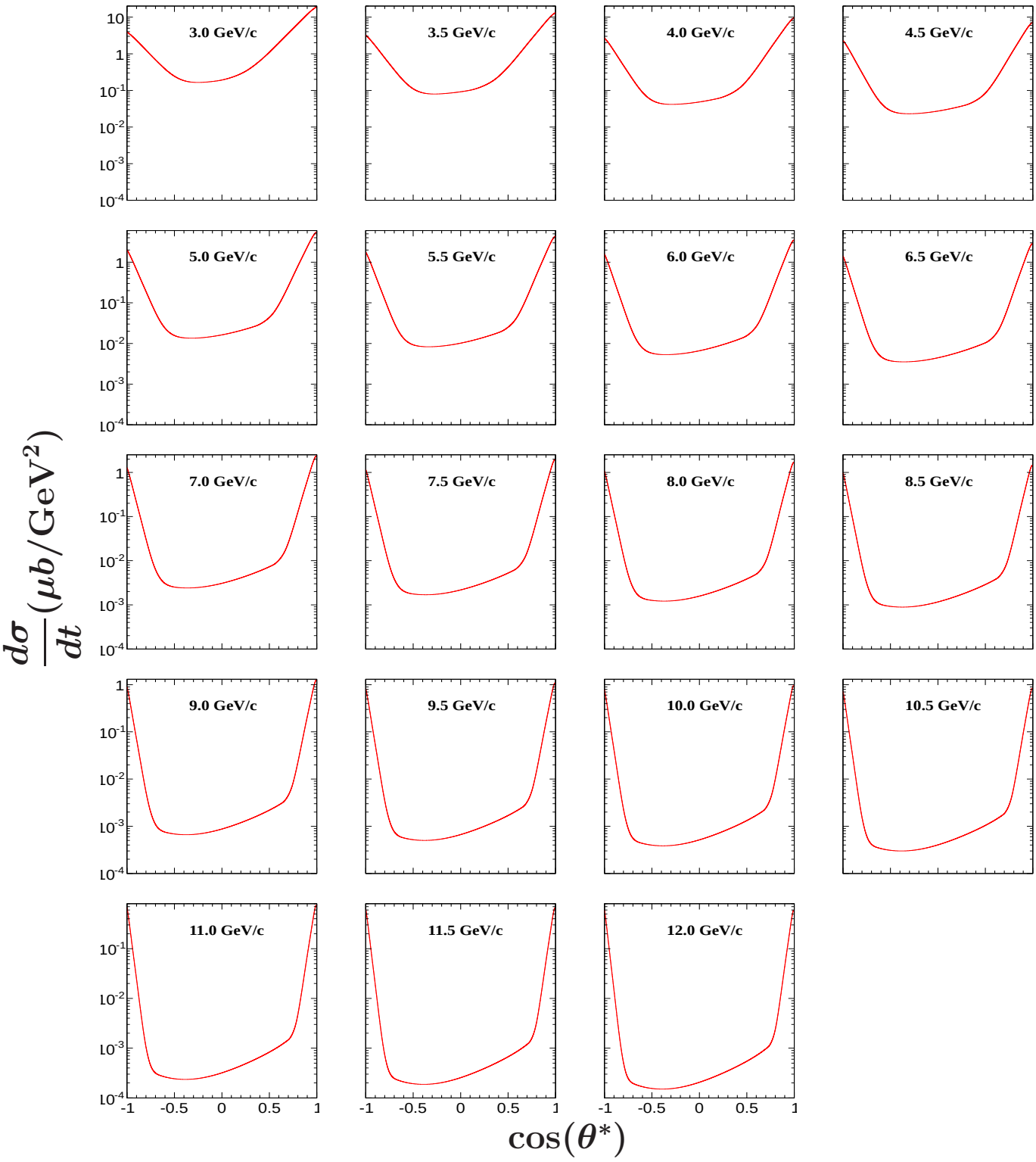

Figure 6: *Differential cross section for the process* $\bar{p}p \to \pi^+\pi^-$ *per unit of the Mandelstam variable* t *as a function of* $\cos\theta^*$ *in the* $\bar{p}p$ *center of mass frame, for antiproton momentum in the lab frame from* 3.0 *GeV to* 12.0 *GeV.*

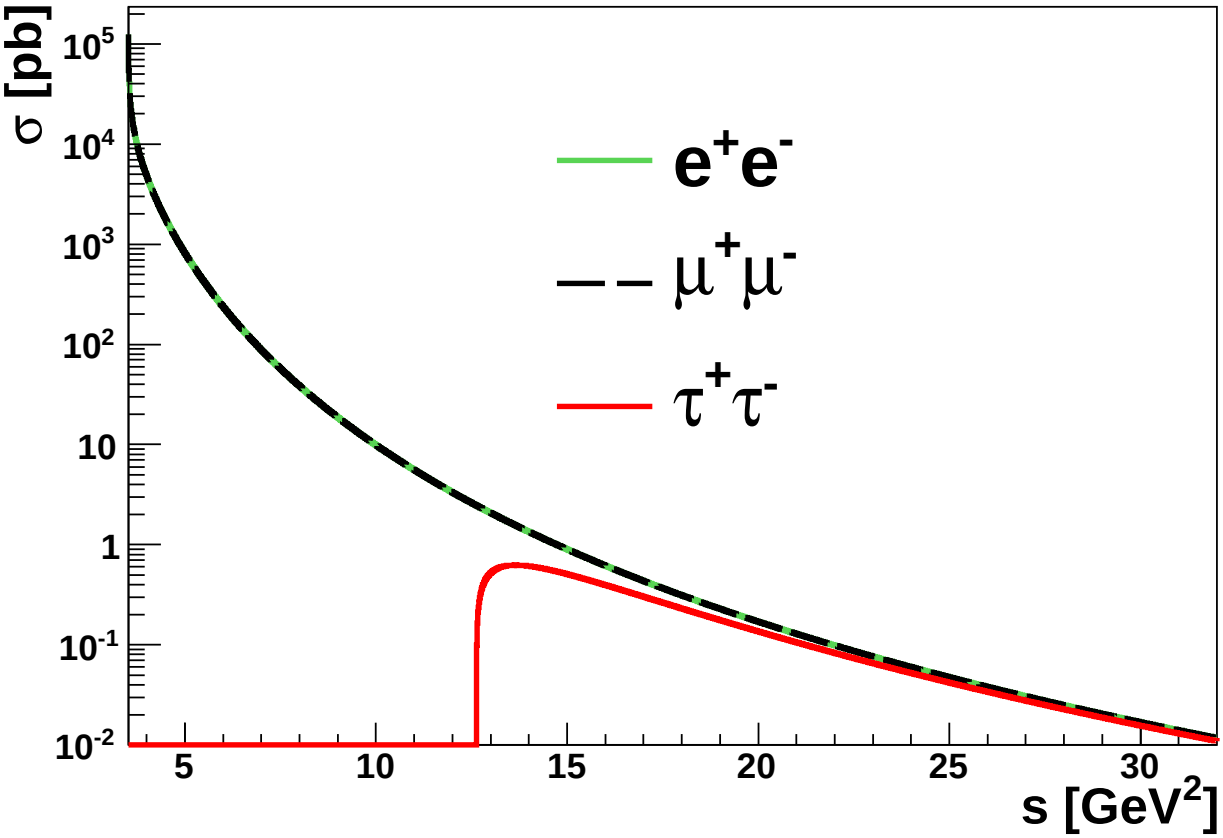

Figure 7: *The integrated cross section in the full angular range* $-1 < \cos\theta^* < 1$ *for* e^+e^- *(green),* $\mu^+\mu^-$ *(black) and* $\tau^+\tau^-$ *(red) production, as a function of the* $\bar{p}p$ *center of mass energy squared* s*, assuming form factors* $G_E(q^2)$ *and* $G_M(q^2)$ *from the pQCD-inspired model.*

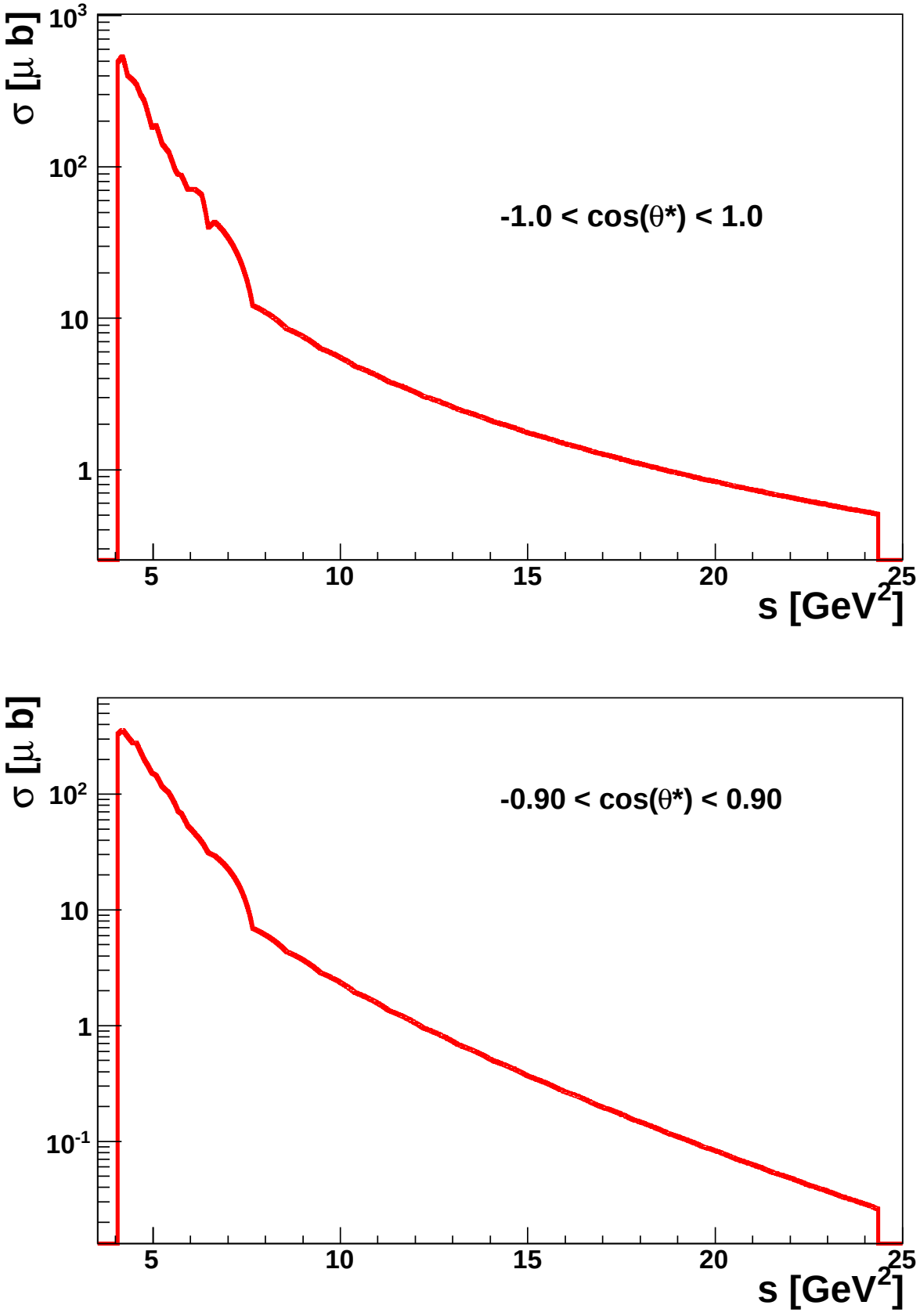

Figure 8: *The integrated cross section for $\pi^+\pi^-$ production in the angular region $-1 < \cos\theta^* < 1$ (top) and $-0.90 < \cos\theta^* < 0.90$ (down), as a function of the $\bar{p}p$ center of mass energy squared s.*

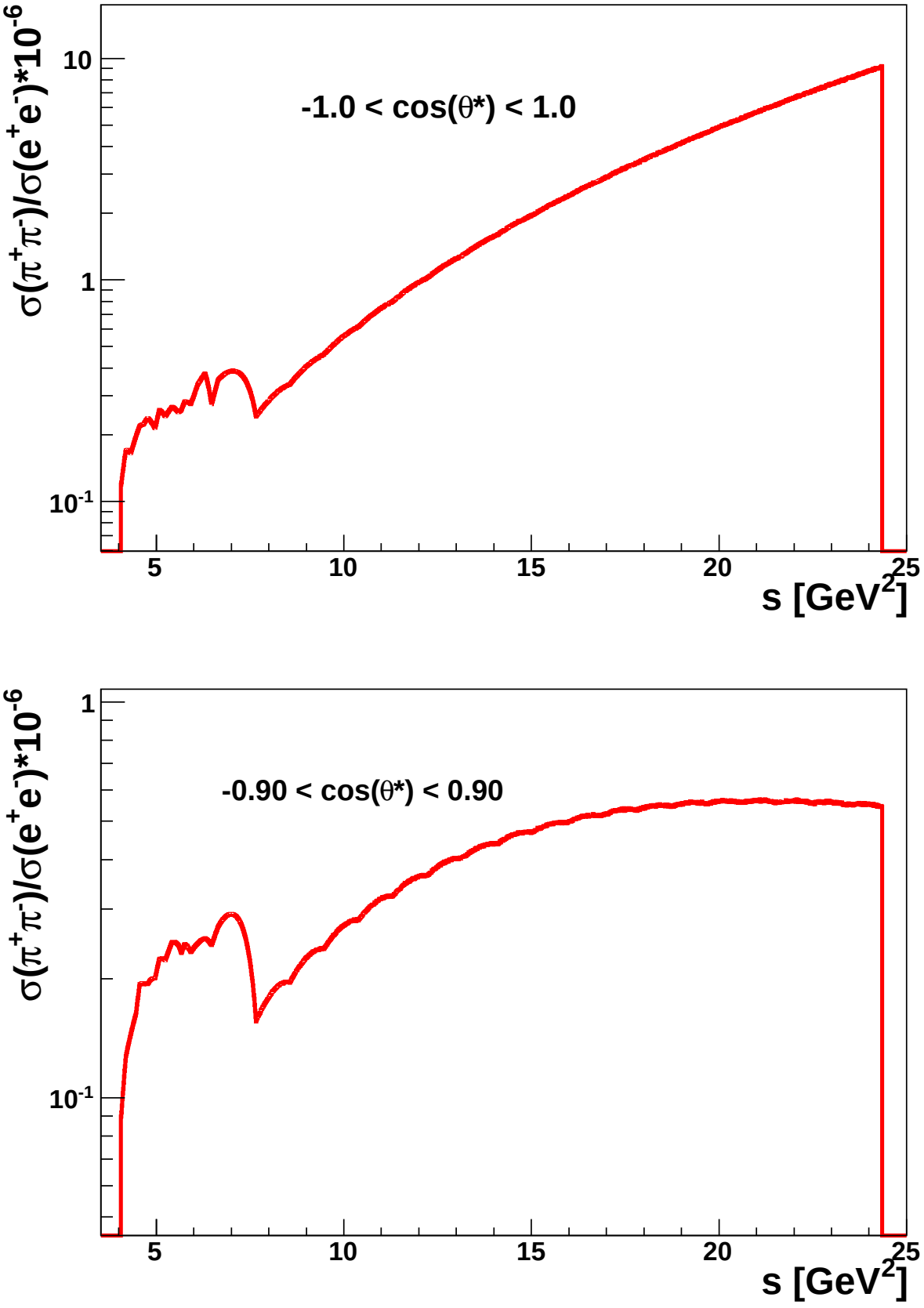

Figure 9: *The ratio of the pion to lepton (electron) integrated cross sections (in units of* 10^6*) in the angular region* $-1 < \cos\theta^* < 1$ *(top) and* $-0.90 < \cos\theta^* < 0.90$ *(down), as a function of the* $\bar{p}p$ *center of mass energy squared* s*. For the lepton cross section, the values of the form factors* $|G_E|$ *and* $|G_M|$ *are taken from the pQCD-inspired model.*

```
-----------------------------------
   Reading infile
-----------------------------------

particle flag:              0
momentum pbar:              3.30 GeV
cos(theta*) min:            -1.00
cos(theta*) max:            1.00
number of bins:             10
FF flag:                    0
ratio GE/GM:                3.00
luminosity:                 2.00 fb^-1
RANLUX seed:                1
number of MC points:        1000000
pathout:                    ../output
outfile:                    mzhistos







PION PRODUCTION: Kinematic regime and cross section parametrization
-------------------------------------------------------------------

 3.00 < P <  5.00 GeV => transition energy regime
cross section parametrization: Regge description


P NOT at lattice site: interpolating cross section between momenta  3.00 and  3.50 GeV







Initial state kinematics
------------------------

=> CM energy square:        S =  8.20 GeV^2
   CM energy:         sqrt(S) =  2.86 GeV
```


Figure 10: *Example output.log file (part 1)*

```
TOTAL CROSS SECTION
===================

−1.00 < cos(theta*) < 1.00
GE, GM from FF model
q2 = 8.20 GeV^2

GE = 0.0440
GM = 0.0440

 => GE/GM = 1.0000

sigma(e+e−)   =  33.02065592                              [pb]
sigma(pi+pi−) =  10.17569261  +/−   0.01857744 (0.18 %) [micro b]

N(e+e−)   =        66041
N(pi+pi−) =  20351385216

sigma(pi+pi−)/sigma(e+e−)*10^{−6}  =   0.30816143

BIN−INTEGRATED CROSS SECTION
============================

−1.00 < cos(theta*) < 1.00,    #bins = 10    =>   cos(theta*) bin width:  a = 0.20
GE, GM from FF model

cos(theta*) bin     sigma(e+e−) [pb]     sigma(pi+pi−) [micro b]      error [micro b]     error [%]         ratio*10^{−6}
---------------     ----------------     -----------------------      ---------------     ----------        -------------
−1.00    −0.80         3.86034351             1.25397467               0.00045853       0.03656586          0.32483500
−0.80    −0.60         3.48815823             0.32780510               0.00012320       0.03758293          0.09397656
−0.60    −0.40         3.20901927             0.10722799               0.00002415       0.02252184          0.03341457
−0.40    −0.20         3.02292663             0.07171337               0.00000196       0.00272879          0.02372316
−0.20    0.00          2.92988031             0.07513733               0.00000295       0.00393083          0.02564519
0.00     0.20          2.92988031             0.09468527               0.00000953       0.01006871          0.03231711
0.20     0.40          3.02292663             0.16523636               0.00003734       0.02259554          0.05466106
0.40     0.60          3.20901927             0.46320527               0.00015988       0.03451538          0.14434481
0.60     0.80          3.48815823             1.67221640               0.00062153       0.03716788          0.47939809
0.80     1.00          3.86034351             5.96525735               0.00200834       0.03366724          1.54526594

sum_{i} sigma(e+e−)[i]   =  33.02065592                                [pb]
sum_{i} sigma(pi+pi−)[i] =  10.19645912   +/−   0.00216166 (0.02 %) [micro b]

cos(theta*) bin     sigma(e+e−)/a [pb]     sigma(pi+pi−)/a [micro b]      error [micro b]     error [%]         ratio*10^{−6}
---------------     ------------------     -------------------------      ---------------     ----------        -------------
−1.00    −0.80         19.30171755                6.26987335               0.00229263       0.03656586          0.32483500
−0.80    −0.60         17.44079116                1.63902551               0.00061599       0.03758293          0.09397656
−0.60    −0.40         16.04509636                0.53613996               0.00012075       0.02252184          0.03341457
−0.40    −0.20         15.11463316                0.35856687               0.00000978       0.00272879          0.02372316
−0.20    0.00          14.64940156                0.37568666               0.00001477       0.00393083          0.02564519
0.00     0.20          14.64940156                0.47342636               0.00004767       0.01006871          0.03231711
0.20     0.40          15.11463316                0.82618181               0.00018668       0.02259554          0.05466106
0.40     0.60          16.04509636                2.31602634               0.00079939       0.03451538          0.14434481
0.60     0.80          17.44079116                8.36108201               0.00310764       0.03716788          0.47939809
0.80     1.00          19.30171755               29.82628674               0.01004169       0.03366724          1.54526594
```


Figure 11: *Example output.log file (part 2)*

```
TOTAL CROSS SECTION
===================

-1.00 < cos(theta*) < 1.00
GM from FF model, GE=R*GM, R user-defined ratio GE/GM
q2 = 8.20 GeV^2

GE = 0.1321
GM = 0.0440

 => GE/GM = 3.0000

sigma(e+e-)   =  79.72181058                              [pb]
sigma(pi+pi-) =  10.17569261  +/-   0.01857744 (0.18 %) [micro b]

N(e+e-)   =       159444
N(pi+pi-) =  20351385216

sigma(pi+pi-)/sigma(e+e-)*10^{-6}  =   0.12764001

BIN-INTEGRATED CROSS SECTION
============================

-1.00 < cos(theta*) < 1.00,    #bins = 10    =>   cos(theta*) bin width:  a = 0.20
GM from FF model, GE=R*GM, R  user-defined ratio GE/GM

cos(theta*) bin     sigma(e+e-) [pb]     sigma(pi+pi-) [micro b]      error [micro b]     error [%]         ratio*10^{-6}
---------------     ----------------     -----------------------      ---------------     ----------        -------------
-1.00    -0.80         5.16797648             1.25397467               0.00045853       0.03656586          0.24264326
-0.80    -0.60         7.03744620             0.32780510               0.00012320       0.03758293          0.04658012
-0.60    -0.40         8.43954849             0.10722799               0.00002415       0.02252184          0.01270542
-0.40    -0.20         9.37428334             0.07171337               0.00000196       0.00272879          0.00765001
-0.20    0.00          9.84165077             0.07513733               0.00000295       0.00393083          0.00763463
0.00     0.20          9.84165077             0.09468527               0.00000953       0.01006871          0.00962087
0.20     0.40          9.37428334             0.16523636               0.00003734       0.02259554          0.01762656
0.40     0.60          8.43954849             0.46320527               0.00015988       0.03451538          0.05488508
0.60     0.80          7.03744620             1.67221640               0.00062153       0.03716788          0.23761694
0.80     1.00          5.16797648             5.96525735               0.00200834       0.03366724          1.15427332

sum_{i} sigma(e+e-)[i]   =  79.72181058                                [pb]
sum_{i} sigma(pi+pi-)[i] =  10.19645912   +/-   0.00216166 (0.02 %) [micro b]

cos(theta*) bin     sigma(e+e-)/a [pb]     sigma(pi+pi-)/a [micro b]      error [micro b]     error [%]         ratio*10^{-6}
---------------     ------------------     -------------------------      ---------------     ----------        -------------
-1.00    -0.80         25.83988242                6.26987335               0.00229263       0.03656586          0.24264326
-0.80    -0.60         35.18723100                1.63902551               0.00061599       0.03758293          0.04658012
-0.60    -0.40         42.19774243                0.53613996               0.00012075       0.02252184          0.01270542
-0.40    -0.20         46.87141672                0.35856687               0.00000978       0.00272879          0.00765001
-0.20    0.00          49.20825387                0.37568666               0.00001477       0.00393083          0.00763463
0.00     0.20          49.20825387                0.47342636               0.00004767       0.01006871          0.00962087
0.20     0.40          46.87141672                0.82618181               0.00018668       0.02259554          0.01762656
0.40     0.60          42.19774243                2.31602634               0.00079939       0.03451538          0.05488508
0.60     0.80          35.18723100                8.36108201               0.00310764       0.03716788          0.23761694
0.80     1.00          25.83988242               29.82628674               0.01004169       0.03366724          1.15427332
```


Figure 12: *Example output.log file (part 3)*

```
<TCanvas::MakeDefCanvas>: created default TCanvas with name c1



Writing histos to file:
     ../output/mzhistos.root   (root file)


HISTOGRAM DESCRIPTION
====================

h0  -> dsigma(e+e-)/dcos(theta*), GE and GM from FF model
h1  -> dsigma(pi+pi-)/dcos(theta*)
h2  -> dsigma(pi+pi-)/dsigma(e^+e^-)*10^{-6}, GE and GM from FF model

h10 -> sigma(e+e-)[i], GE and GM from FF model
h11 -> sigma(pi+pi-)[i]
h12 -> sigma(pi+pi-)[i]/sigma(e+e-)[i]*10^{-6}, GE and GM from FF model
h14 -> sigma(e+e-)[i]/a, a=bin width, GE and GM from FF model
h15 -> sigma(pi+pi-)[i]/a, a=bin width

h100  -> dsigma(e+e-)/dcos(theta*), GM from FF model, GE=R*GM, R user-defined ratio GE/GM
h102  -> dsigma(pi+pi-)/dsigma(e^+e^-)*10^{-6}, GM from FF model, GE=R*GM, R user-defined ratio GE/GM

h110 -> sigma(e+e-)[i], GM from FF model, GE=R*GM, R user-defined ratio GE/GM
h112 -> sigma(pi+pi-)[i]/sigma(e+e-)[i]*10^{-6}, GM from FF model, GE=R*GM, R user-defined ratio GE/GM
h114 -> sigma(e+e-)[i]/a, a=bin width, GM from FF model, GE=R*GM, R user-defined ratio GE/GM



Execution time... 8.97s
```

Figure 13: *Example output.log file (part 4)*

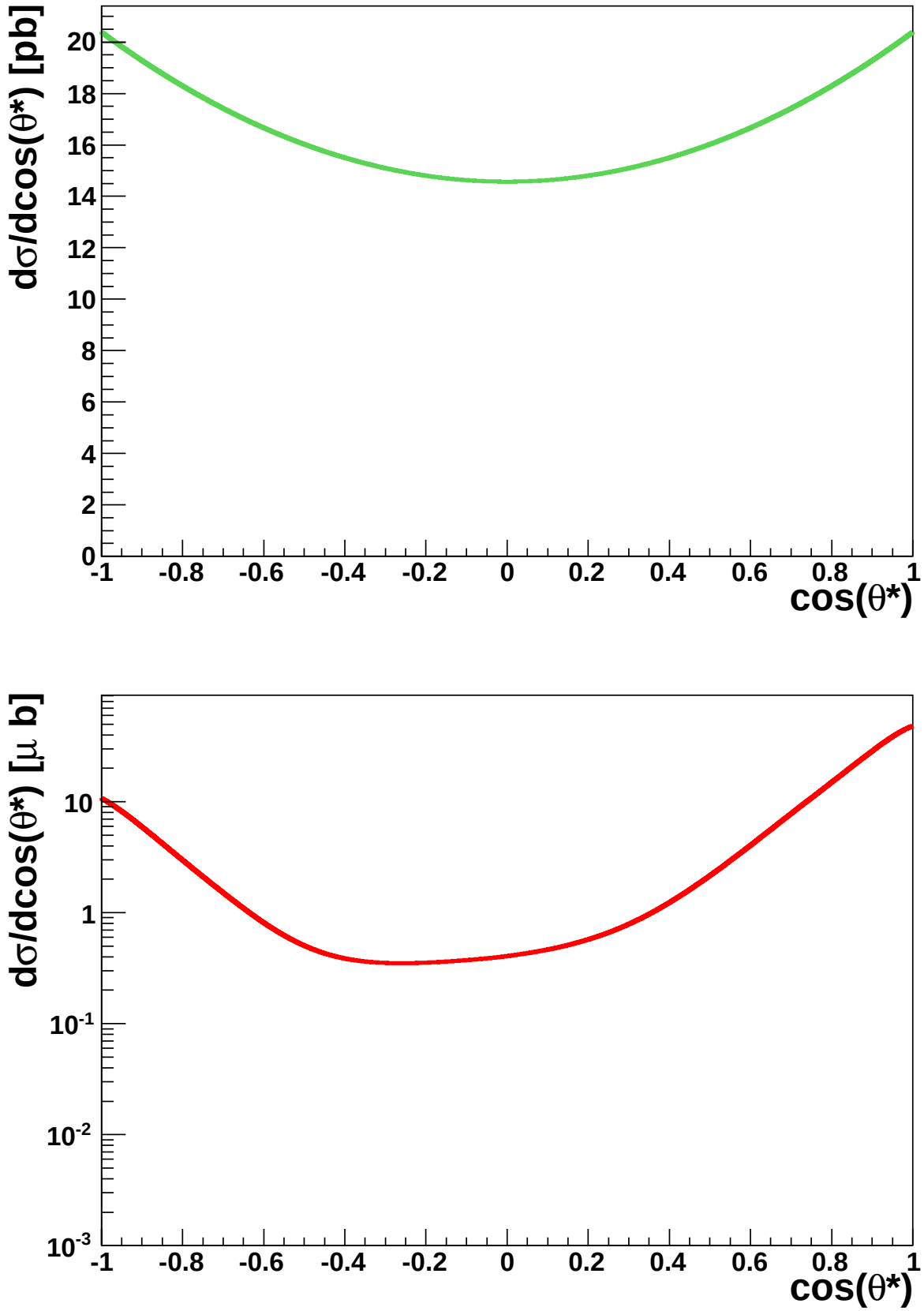

Figure 14: *The differential cross section* $d\sigma/d\cos\theta^*$ *for* $\bar{p}p \to e^+e^-$ *(top) and* $\bar{p}p \to \pi^+\pi^-$ *(down) for antiproton momentum* $P = 3.3$ *GeV as a function of* $\cos\theta^*$*, in the region* $-1 < \cos\theta^* < 1$*. For lepton production, the values of the form factors* $|G_E|$ *and* $|G_M|$ *are taken from the pQCD-inspired model.*

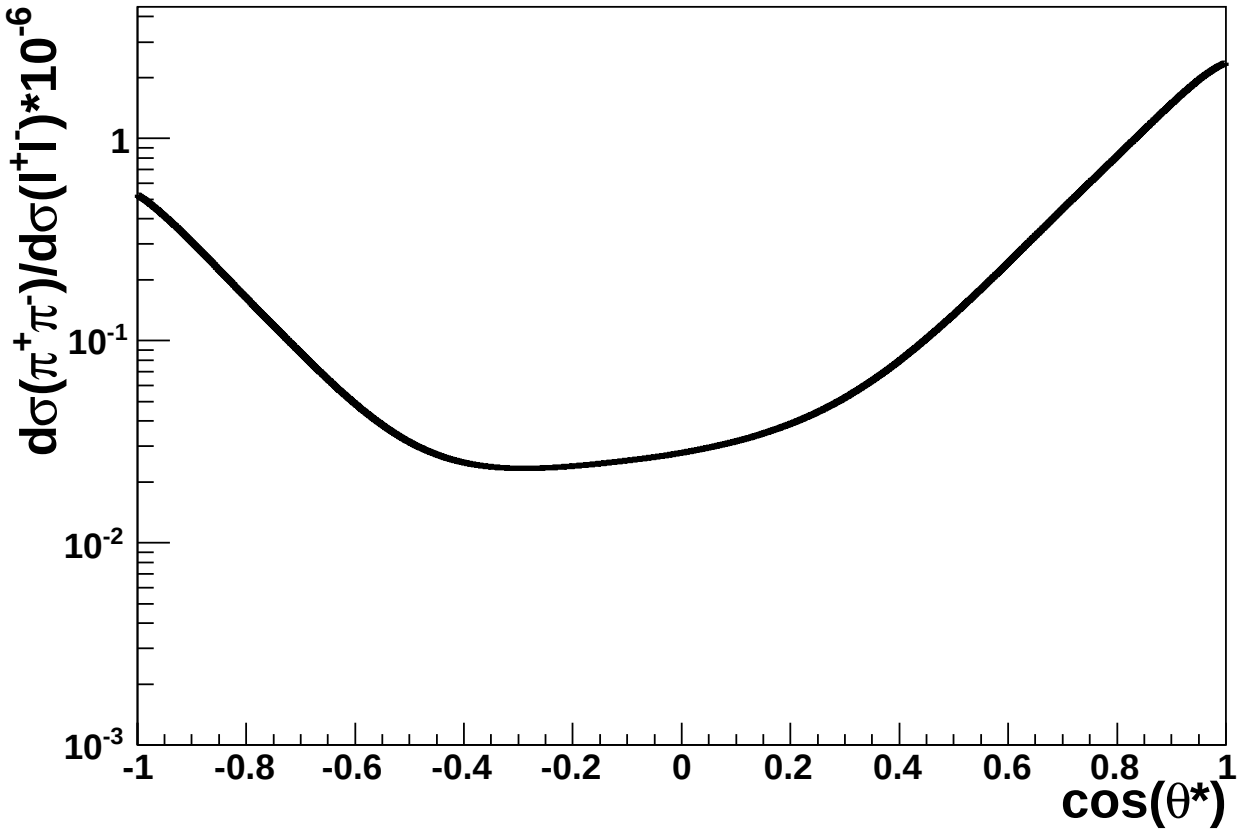

Figure 15: *The ratio* $d\sigma(\bar{p}p \to \pi^+\pi^-)/d\sigma(\bar{p}p \to e^+e^-)$ *(in units of* 10^6*), for antiproton momentum* $P = 3.3$ *GeV as a function of* $\cos\theta^*$*, in the region* $-1 < \cos\theta^* < 1$*. For lepton production, the values of the form factors* $|G_E|$ *and* $|G_M|$ *are taken from the pQCD-inspired model.*

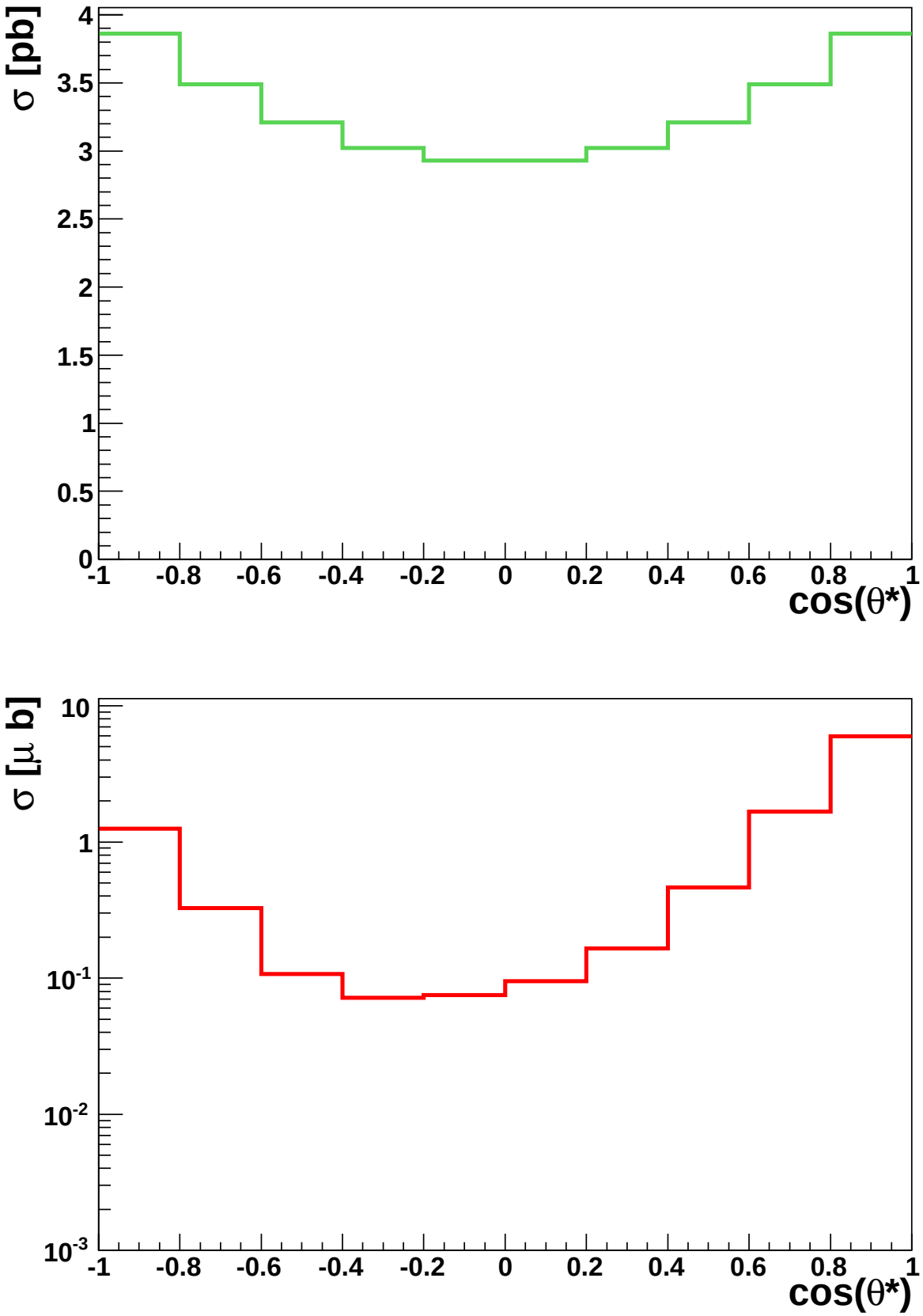

Figure 16: *The bin-integrated cross section $\sigma(\bar{p}p \to e^+e^-)$ (top) and $\sigma(\bar{p}p \to \pi^+\pi^-)$ (down) for antiproton momentum $P = 3.3$ GeV, in the region $-1 < \cos\theta^* < 1$, with a total of 10 $\cos\theta^*$ bins. For lepton production, the values of the form factors $|G_E|$ and $|G_M|$ are taken from the pQCD-inspired model.*

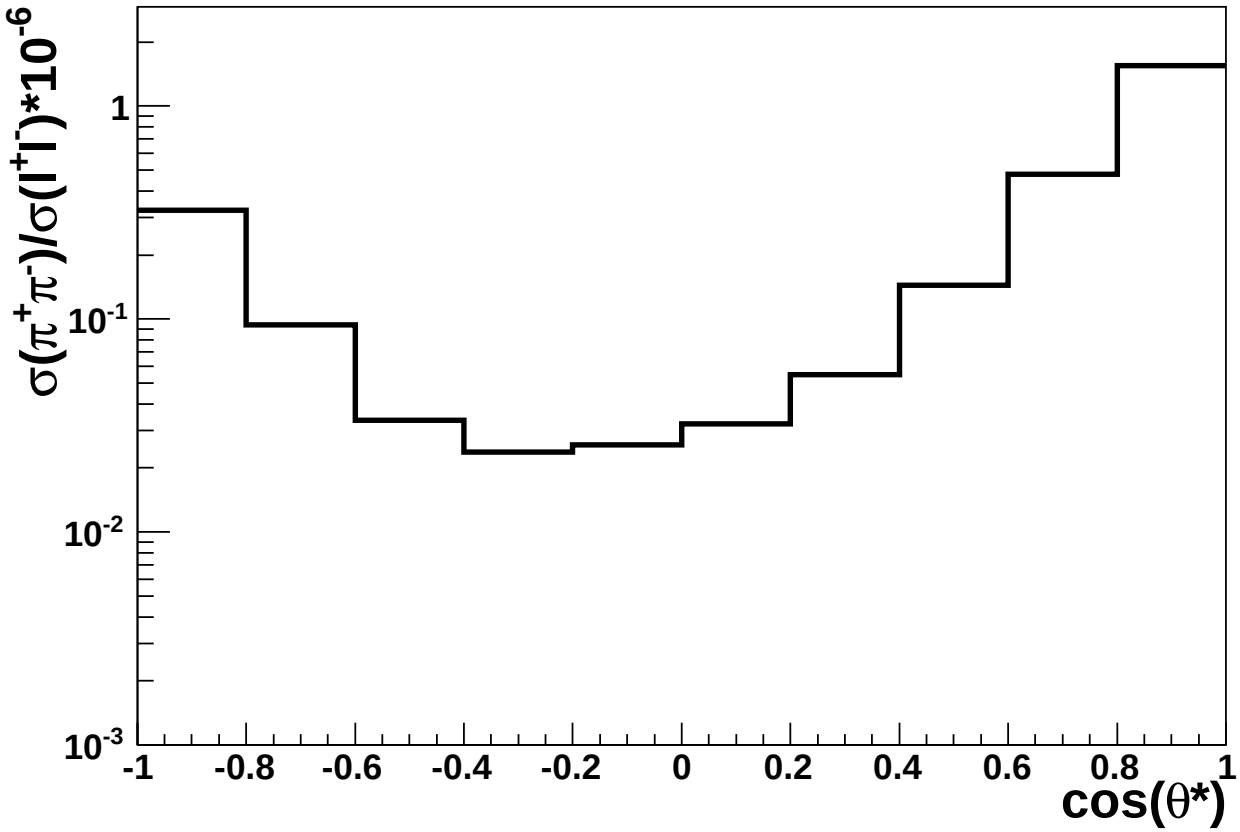

Figure 17: *The bin-integrated cross section ratio $\sigma(\bar{p}p \to \pi^+\pi^-)/\sigma(\bar{p}p \to e^+e^-)$ (in units of 10^6), for antiproton momentum $P = 3.3$ GeV, in the region $-1 < \cos\theta^* < 1$, with a total of $10\ \cos\theta^*$ bins. For lepton production, the values of the form factors $|G_E|$ and $|G_M|$ are taken from the pQCD-inspired model.*

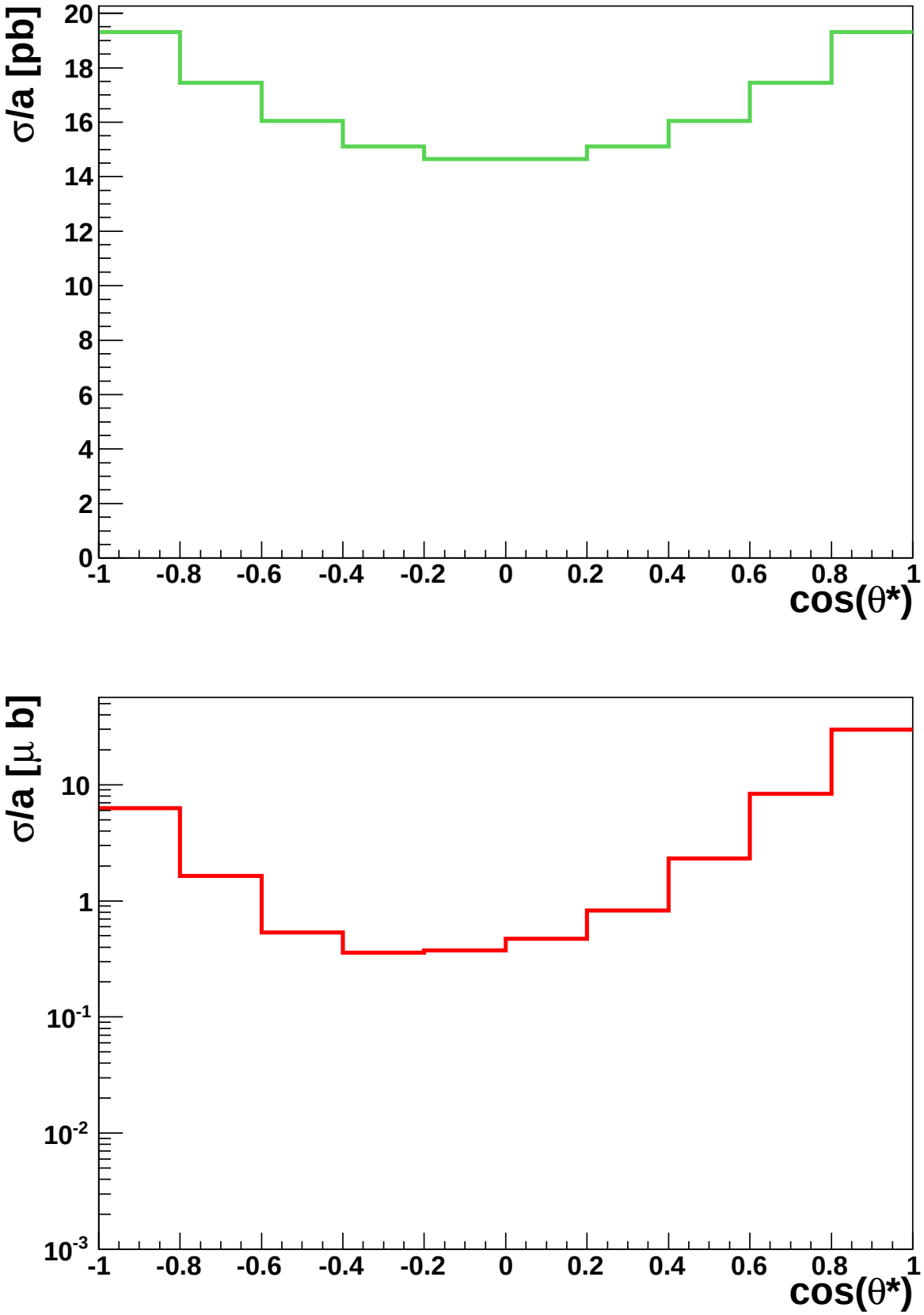

Figure 18: *The bin-integrated cross section $\sigma(\bar{p}p \to e^+e^-)$ (top) and $\sigma(\bar{p}p \to \pi^+\pi^-)$ (down) divided by the bin width $a = 0.20$ for antiproton momentum $P = 3.3$ GeV, in the region $-1 < \cos\theta^* < 1$, with a total of 10 $\cos\theta^*$ bins. For lepton production, the values of the form factors $|G_E|$ and $|G_M|$ are taken from the pQCD-inspired model.*

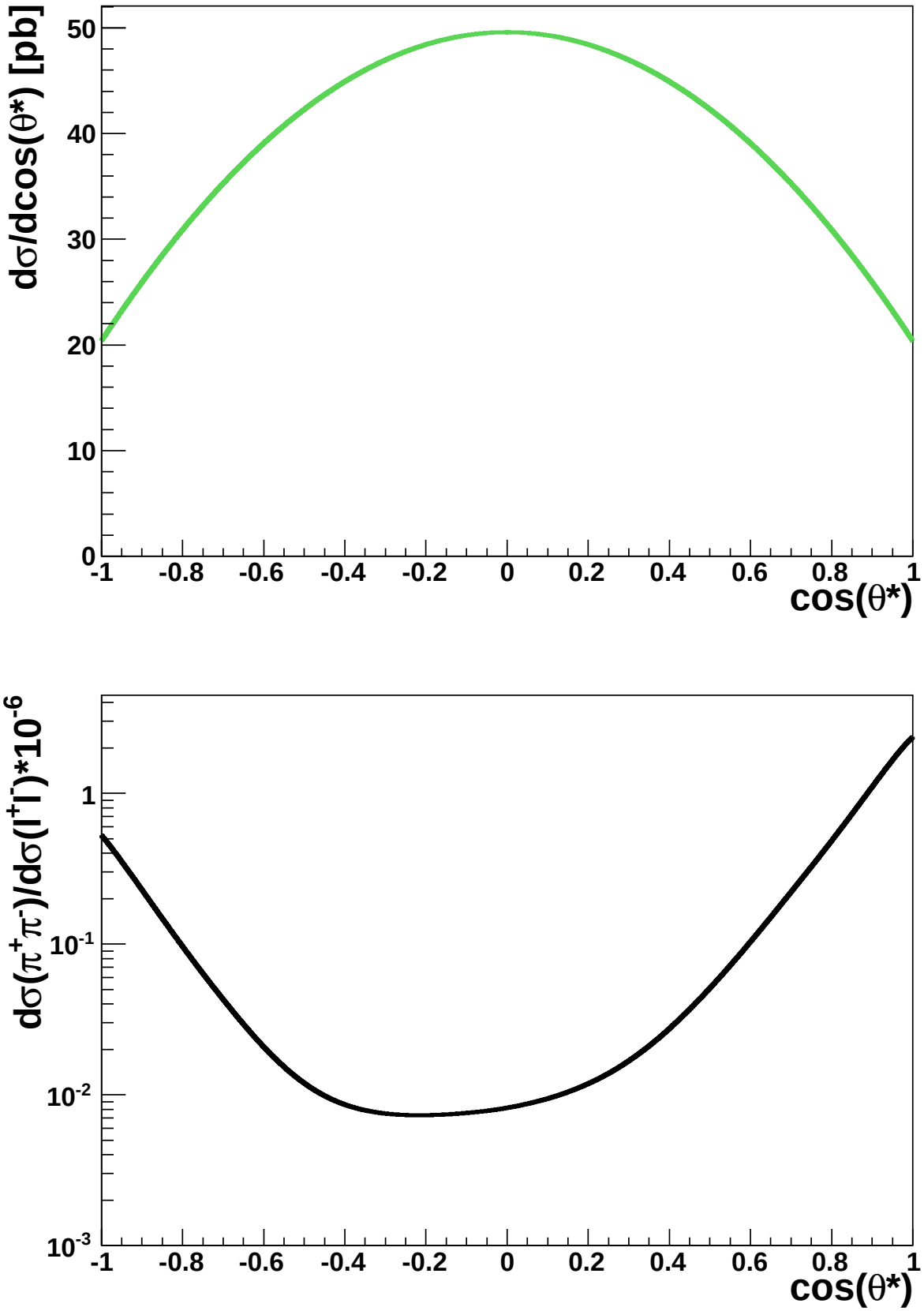

Figure 19: *The differential cross section* $d\sigma/d\cos\theta^*$ *for* $\bar{p}p \to e^+e^-$ *(top) and the ratio* $d\sigma(\bar{p}p \to \pi^+\pi^-)/d\sigma(\bar{p}p \to e^+e^-)$ *(down) for antiproton momentum* $P = 3.3$ *GeV as a function of* $\cos\theta^*$*, in the region* $-1 < \cos\theta^* < 1$*. For lepton production, the value of the form factor* $|G_M|$ *is taken from the pQCD-inspired model, whereas the form factor* $|G_E|$ *is set to* $|G_E| = R \cdot |G_M|$*, with* $R = 3$*.*

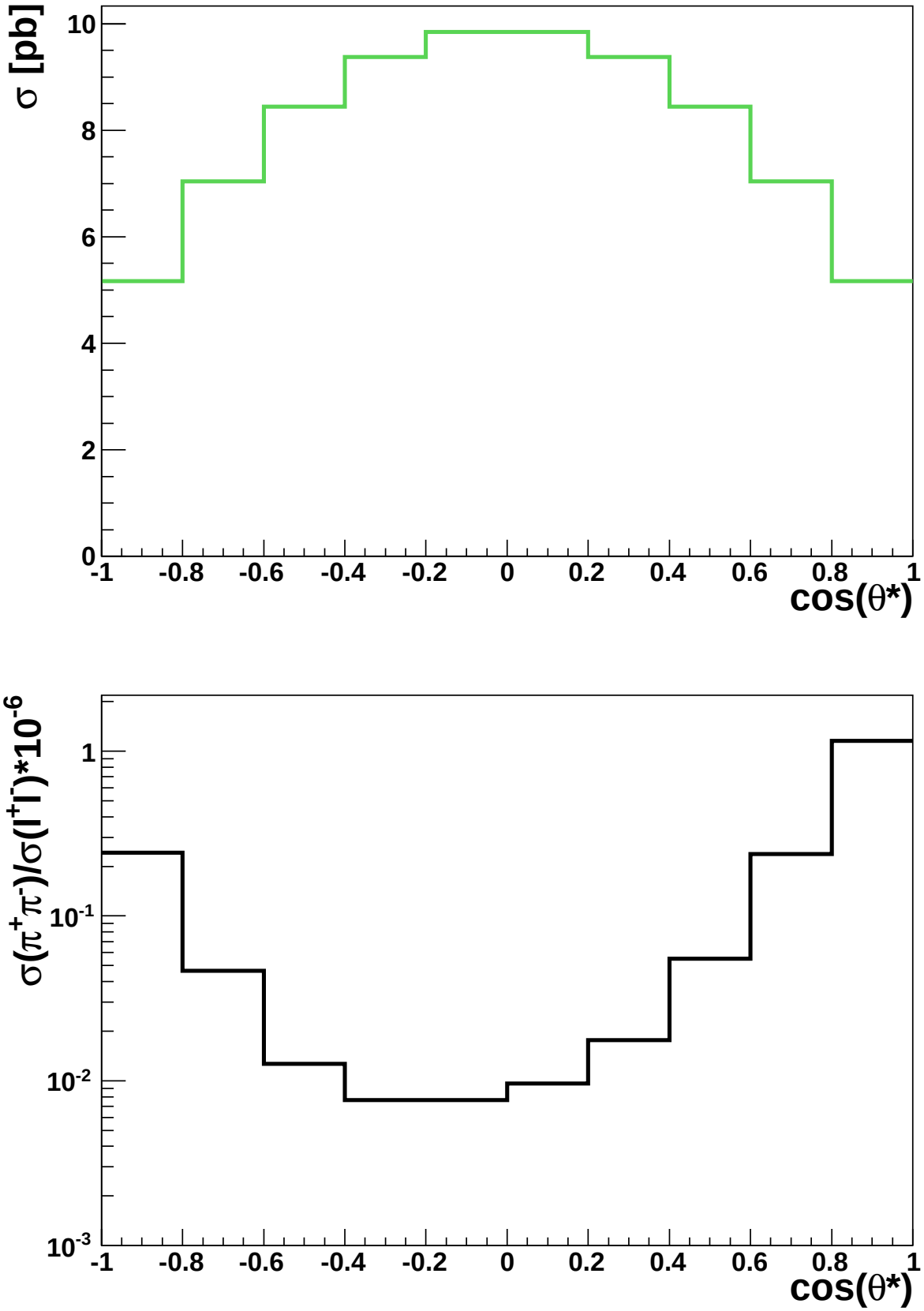

Figure 20: *The bin-integrated cross section* $\sigma(\bar{p}p \to e^+e^-)$ *(top) and ratio* $\sigma(\bar{p}p \to \pi^+\pi^-)/\sigma(\bar{p}p \to e^+e^-)$ *(in units of* 10^6*) (down), for antiproton momentum* $P = 3.3$ *GeV, in the region* $-1 < \cos\theta^* < 1$*, with a total of* $10\ \cos\theta^*$ *bins. For lepton production, the value of the form factor* $|G_M|$ *is taken from the pQCD-inspired model, whereas the form factor* $|G_E|$ *is set to* $|G_E| = R \cdot |G_M|$*, with* $R = 3$*.*

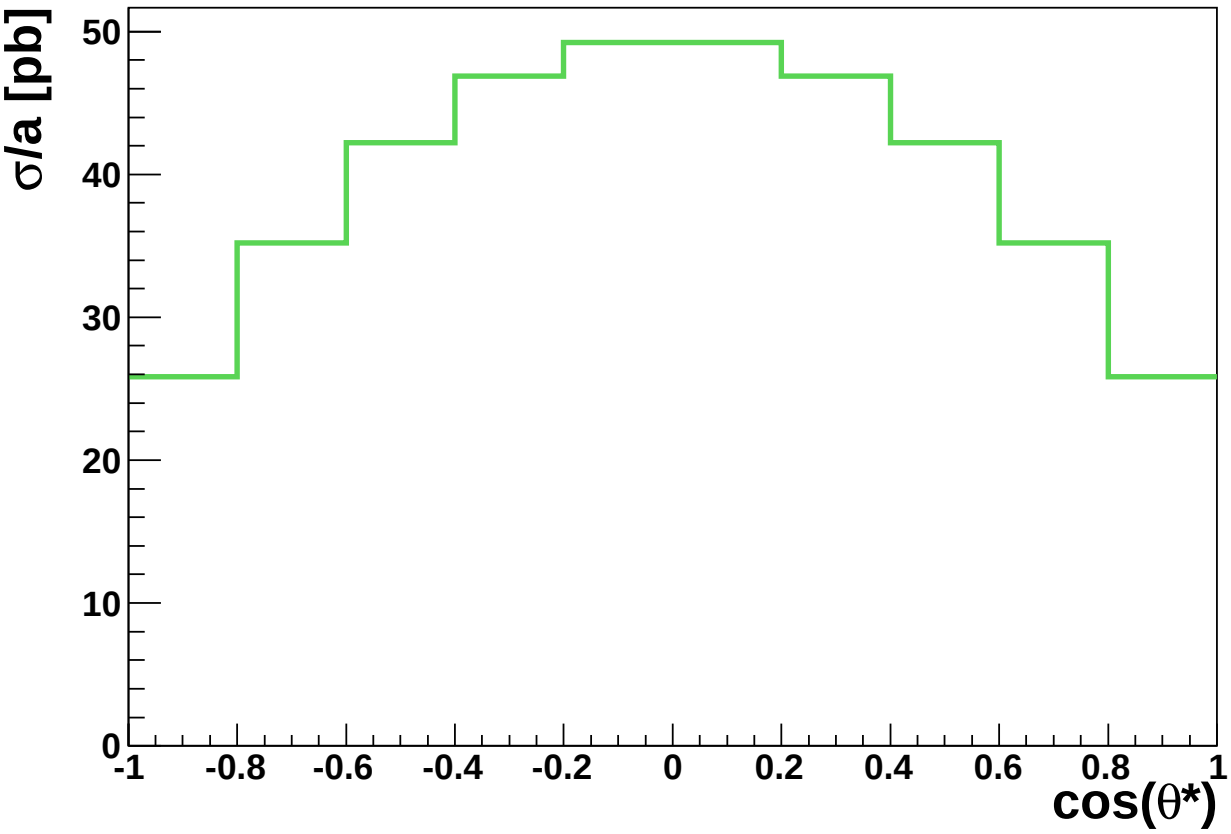

Figure 21: *The bin-integrated cross section* $\sigma(\bar{p}p \to e^+e^-)$ *divided by the bin width* $a = 0.20$ *for antiproton momentum* $P = 3.3$ *GeV, in the region* $-1 < \cos\theta^* < 1$*, with a total of* $10\ \cos\theta^*$ *bins. The value of the form factor* $|G_M|$ *is taken from the pQCD-inspired model, whereas the form factor* $|G_E|$ *is set to* $|G_E| = R \cdot |G_M|$*, with* $R = 3$*.*